


# Electrochemical properties of the non-excitable tissue stria vascularis of the mammalian cochlea are sensitive to sounds

Qi Zhang<sup>1,2,3</sup>, Takeru Ota<sup>1</sup>, Takamasa Yoshida<sup>4</sup>, Daisuke Ino<sup>1</sup>, Mitsuo P. Sato<sup>5</sup>, Katsumi Doi<sup>5</sup>, Arata Horii<sup>3</sup>, Fumiaki Nin<sup>6</sup> and Hiroshi Hibino<sup>1,7</sup> 

<sup>1</sup>Division of Global Pharmacology, Department of Pharmacology, Graduate School of Medicine, Osaka University, Suita, Osaka, Japan

<sup>2</sup>Department of Molecular Physiology, Niigata University Graduate School of Medical and Dental Sciences, Asahimachi-dori, Niigata, Japan

<sup>3</sup>Department of Otolaryngology Head and Neck Surgery, Niigata University Graduate School of Medical and Dental Sciences, Asahimachi-dori, Niigata, Japan

<sup>4</sup>Department of Otorhinolaryngology, Graduate School of Medical Sciences, Kyushu University, Maidashi, Fukuoka, Japan

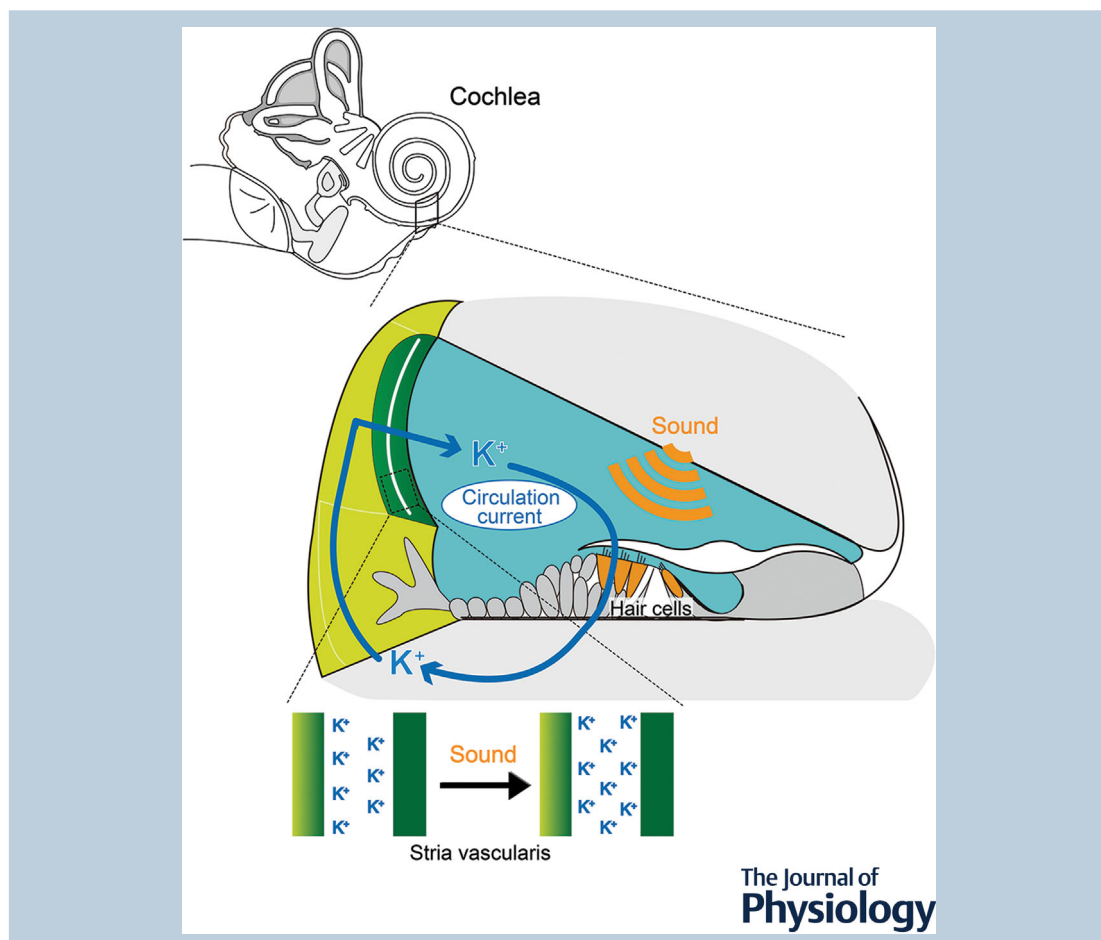
<sup>5</sup>Department of Otolaryngology, Kindai University Faculty of Medicine, Osaka, Japan

<sup>6</sup>Department of Physiology, Division of Biological Principles, Graduate School of Medicine, Gifu University, Yanagido, Gifu, Japan

<sup>7</sup>AMED, AMED-CREST, Osaka, Japan

Edited by: Ian Forsythe & Walter Marcotti

The peer review history is available in the supporting information section of this article (<https://doi.org/10.1113/JP281981#support-information-section>).



Qi Zhang and Takeru Ota contributed equally to this work.

**Abstract** Excitable cochlear hair cells convert the mechanical energy of sounds into the electrical signals necessary for neurotransmission. The key process is cellular depolarization via  $K^+$  entry from  $K^+$ -enriched endolymph through hair cells' mechanosensitive channels. Positive 80 mV potential in endolymph accelerates the  $K^+$  entry, thereby sensitizing hearing. This potential represents positive extracellular potential within the epithelial-like stria vascularis; the latter potential stems from  $K^+$  equilibrium potential ( $E_K$ ) across the strial membrane. Extra- and intracellular  $[K^+]$  determining  $E_K$  are likely maintained by continuous unidirectional circulation of  $K^+$  through a putative  $K^+$  transport pathway containing hair cells and stria. Whether and how the non-excitable tissue stria vascularis responds to acoustic stimuli remains unclear. Therefore, we analysed a cochlear portion for the best frequency, 1 kHz, by theoretical and experimental approaches. We have previously developed a computational model that integrates ion channels and transporters in the stria and hair cells into a circuit and described a circulation current composed of  $K^+$ . Here, in this model, mimicking of hair cells'  $K^+$  flow induced by a 1 kHz sound modulated the circulation current and affected the strial ion transport mechanisms; the latter effect resulted in monotonically decreasing potential and increasing  $[K^+]$  in the extracellular strial compartment. Similar results were obtained when the stria in acoustically stimulated animals was examined using microelectrodes detecting the potential and  $[K^+]$ . Measured potential dynamics mirrored the  $E_K$  change. Collectively, because stria vascularis is electrically coupled to hair cells by the circulation current *in vivo* too, the strial electrochemical properties respond to sounds.

(Received 4 June 2021; accepted after revision 18 August 2021; first published online 23 August 2021)

**Corresponding author** Hiroshi Hibino: Division of Global Pharmacology, Department of Pharmacology, Graduate School of Medicine, Osaka University, 2-2 Yamadaoka, Suita, Osaka 565-0871, Japan. Email: hibino@pharma2.med.osaka-u.ac.jp

Fumiaki Nin: Department of Physiology, Division of Biological Principles, Graduate School of Medicine, Gifu University, 1-1 Yanagido, Gifu 501-1112, Japan. Email: nin@gifu-u.ac.jp

**Abstract figure legend** Evidence for functional linkage between a double-layered epithelial-like tissue, stria vascularis, and sensory hair cells in the cochlea of the mammalian inner ear. The endolymph, which is highlighted by blue in the cochlear cross section, exhibits a highly positive potential of +80 mV. This potential is essential for the excitation of hair cells and is dependent upon the  $[K^+]$  homeostasis in the extracellular space in the stria. The  $[K^+]$  balance is likely to be maintained by 'circulation current', a radial ionic flow in the cochlea. Not only computational simulation but also *in vivo* electrophysiological experiments using guinea pigs showed that stimulation of the hair cells by sounds changed the strial  $[K^+]$  property. This result indicates that the circulation current electrically couples the stria vascularis to the hair cells.

### Key points

- A highly positive potential of +80 mV in  $K^+$ -enriched endolymph in the mammalian cochlea accelerates sound-induced  $K^+$  entry into excitable sensory hair cells, a process that triggers hearing.
- This unique endolymphatic potential represents an  $E_K$ -based battery for a non-excitable epithelial-like tissue, the stria vascularis.
- To examine whether and how the stria vascularis responds to sounds, we used our computational model, in which strial channels and transporters are serially connected to those hair cells in a closed-loop circuit, and found that mimicking hair cell excitation by acoustic stimuli resulted in increased extracellular  $[K^+]$  and decreased the battery's potential within the stria.
- This observation was overall verified by electrophysiological experiments using live guinea pigs.
- The sensitivity of electrochemical properties of the stria to sounds indicates that this tissue is electrically coupled to hair cells by a radial ionic flow called a circulation current.

## Introduction

Mammalian hearing can perceive extremely faint sounds of approximately 20  $\mu\text{Pa}$ . Such high sensitivity stems primarily from the function of the cochlea in the inner ear (Fig. 1A). A key element is the sensory epithelium, which can respond to vibrations of only  $\pm 0.3$  nm induced by threshold acoustic stimulation (Hudspeth, 1997). This performance depends not only on the active processes observed in sensory hair cells, which are excitable cells in the epithelium, but also on the unique electrochemical environment in the cochlea (Davis, 1961; Brownell *et al.* 2001; Hibino & Kurachi, 2006; Hudspeth, 2008; Jacob *et al.* 2011). In mammals, endolymph, which fills the scala media, a chamber in the organ, contains high  $[\text{K}^+]$  of 150 mM and low  $[\text{Ca}^{2+}]$  of 20  $\mu\text{M}$ ; in addition, this extracellular solution shows a positive endocochlear potential (EP) of 80–100 mV relative to perilymph in a different chamber, the scala tympani (Fig. 1B) (Békésy, 1952; Smith *et al.* 1954). Hair cells expose the hair bundle composed of stereocilia to endolymph, and their cell bodies are bathed in perilymph, the ionic composition of which resembles that of blood plasma. The tip of the stereocilium expresses mechanoelectrical transduction (MET) channels. The channels, even in a resting state, are open to some extent thereby allowing considerable  $\text{K}^+$  amounts to enter the cells from endolymph. The mechanical force induced by a sound sinusoidally changes the open probability ( $P_o$ ) of MET channels. In this process, deflection of the hair bundle towards the taller stereocilia increases  $P_o$  and augments  $\text{K}^+$  entry into the hair cells, thus depolarizing them (Hudspeth, 1989). The highly positive EP enhances the driving force behind cation influx through the channels and therefore sensitizes hearing. Loss of the EP causes deafness (Schmiedt *et al.* 2002). Under any conditions,  $\text{K}^+$  exits the hair cell into perilymph through voltage-gated channels on the basolateral surface (Kubisch *et al.* 1999). Then, it is assumed to cycle back to endolymph through ion channels and transporters expressed primarily in the stria vascularis (Fig. 1B) (Kikuchi *et al.* 1995; 2000a; Spicer & Schulte, 1996; Wangemann, 2002; 2006). This  $\text{K}^+$  recycling is likely to contribute to  $\text{K}^+$  homeostasis in the cochlea.

A number of studies have shown that the stria vascularis, which is an epithelial-like non-excitable tissue,

in the lateral cochlear wall plays key roles in the formation of the EP (Tasaki & Spyropoulos, 1959; Salt *et al.* 1987; Hibino *et al.* 1997; Wangemann, 2002). In terms of its function, the stria vascularis is thought to consist of two layers: inner and outer (Fig. 1C). The inner one is a single layer of marginal cells in the stria vascularis, and the apical surfaces of these cells face endolymph. The outer layer represents a syncytium composed of intermediate and basal cells in the stria and fibrocytes in a neighbouring tissue: the spiral ligament. These three cell types are intracellularly connected via gap junctions, thereby sharing a similar electrochemical profile (Kikuchi *et al.* 1995; 2000b; Spicer & Schulte, 1996; Takeuchi & Ando, 1998). An extracellular space of  $\sim 15$  nm between the outer layer and inner layer, which is referred to as the intrastrial space (IS), contains numerous capillaries (Fig. 1C) (Hinojosa & Rodriguez-Echandia, 1966). The IS is characterized by low  $[\text{K}^+]$  similar to that of perilymph and a high potential resembling the EP (Salt *et al.* 1987; Ikeda & Morizono, 1989; Nin *et al.* 2008). Under normal conditions, the IS potential (ISP) is a major source of EP and is generated by multiple factors (Fig. 1D) (Salt *et al.* 1987; Ando & Takeuchi, 1999; Takeuchi *et al.* 2000; Nin *et al.* 2008; Adachi *et al.* 2013; Yoshida *et al.* 2016; Nin *et al.* 2016). The apical surface of the outer syncytial layer not only abundantly expresses  $\text{K}^+$  channels, Kir4.1 (see Fig. 1C), but is also exposed to a large  $[\text{K}^+]$  gradient between the IS and the inside of the layer. The cooperation of these two arrangements results in the formation of a large  $\text{K}^+$  equilibrium potential ( $E_K$ ). Moreover, the basolateral surface of the syncytial layer is highly permeable to  $\text{Na}^+$ , even in a resting state, thereby exhibiting a positive resting membrane potential of +5–+12 mV with reference to the perilymph *in vivo* (Yoshida *et al.* 2016). Owing to this unusual electrical property, the transepithelial voltage across the syncytial layer, which is the sum of the membrane potentials on the basolateral and apical surfaces, establishes the ISP, which is again recorded as a highly positive value relative to the perilymph. Notably, the low  $[\text{K}^+]$  in the IS, i.e. the ionic milieu necessary for the  $[\text{K}^+]$  gradient across the apical surface of the outer syncytial layer, is controlled by  $\text{Na}^+$ ,  $\text{K}^+$ -ATPases, and  $\text{Na}^+$ ,  $\text{K}^+$ ,  $2\text{Cl}^-$ -cotransporter on the basolateral surface of the inner layer (Nin *et al.* 2008; 2012; 2017; Yoshida *et al.* 2015). The other key element for maintaining the positive

**Qi Zhang**, a PhD student at the Department of Otolaryngology Head and Neck Surgery, Niigata University, is currently studying as a special student at the Division of Global Pharmacology, Department of Pharmacology, Graduate School of Medicine, Osaka University, Japan. He obtained an MD degree in Clinical Medicine at Harbin Medical University, China. His main research focus is the exploration of the pathophysiological mechanisms underlying inner ear disorders. **Takeru Ota** is an Assistant Professor at the Division of Global Pharmacology, Department of Pharmacology, Graduate School of Medicine, Osaka University. He obtained a BSc degree in Physico-informatics at Keio University in 2009, and received an MSc degree in Physics and a PhD degree in Dentistry in 2011 and 2016, respectively, at Tohoku University. He is currently working on auditory physiology, biophysics, electrophysiology, optical coherence tomography and optoelectronic systems.



potential in the IS is electrical isolation of this extracellular space from the neighbouring perilymph and endolymph (Nin *et al.* 2008). Finally, the  $E_K$  formed by different  $K^+$  channels, KCNQ1/KCNE1, on the apical surface of the inner layer also contributes to the EP (Nin *et al.* 2008; 2012; Hibino *et al.* 2010).

In addition to  $K^+$  recycling theory, a classic model electrically and serially links the stria vascularis, which serves as a battery, to hair cells and involves a continuous current in this closed circuit even in a resting state (Davis, 1953; 1958; 1965). Indeed, a radial standing current was successfully measured *in vivo* by means

of a microelectrode inserted in perilymph and was modulated by acoustic stimuli (Zidanic & Brownell, 1990). Electrophysiological experiments have revealed that the exposure of animals to a sound induces a moderate reduction in the EP (Davis, 1957; Davis *et al.* 1958; Honrubia & Ward, 1969). In spite of this observation and assumptions in conventional models, whether and how acoustic stimuli can affect the electrochemical properties of the stria vascularis remains elusive. We have previously constructed a computational model in which the channels and transporters in the stria vascularis are serially connected with those in hair cells into an electrical

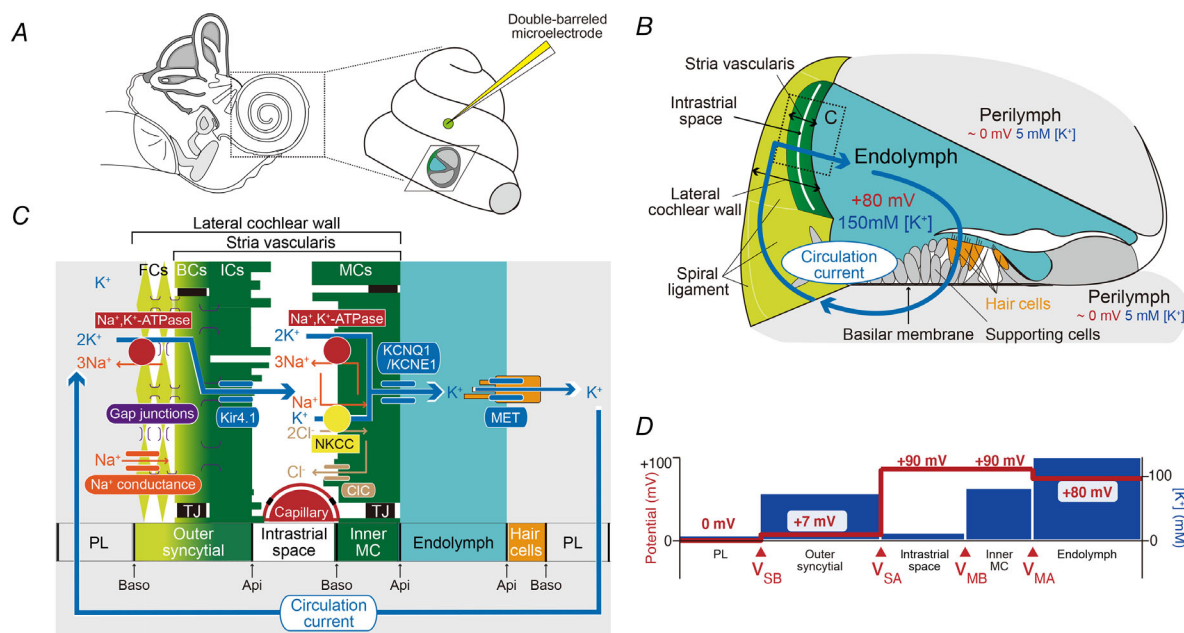


**Figure 1. Morphological and electrochemical characteristics of the cochlea**

**A**, structure of the guinea pig cochlea. The composition of the peripheral auditory organ and the appearance of the cochlea are depicted in left and right panels, respectively. In the latter, a cross-section of the organ is shown and is highlighted by a box. In the electrophysiological experiments of this study, a double-barrelled electrode sensitive to  $[K^+]$  and to the potential was inserted into the central position on the cochlear second turn through a small hole made on the bony wall (right panel). **B**, tissue and cellular components of the cochlea. The schematics correspond to the cross-section presented in the right panel of (A). Illustrated are the lateral cochlear wall composed of the stria vascularis and spiral ligament as well as the sensory epithelium containing hair cells, supporting cells and the basilar membrane. The intrastrial space (IS) is a narrow extracellular space of  $\sim 15$  nm in width in the stria. The potential and  $[K^+]$  in two different extracellular fluids, perilymph and endolymph, are described too. Note that a 'circulation current' is likely to unidirectionally flow along a pathway consisting of endolymph, hair cells, perilymph and the lateral wall. The region highlighted by the *dotted box* is expanded in (C). **C**, cellular constituents of the lateral cochlear wall. The stria vascularis contains marginal cells (MCs), intermediate cells (ICs) and basal cells (BCs). All the ICs, BCs and neighbouring fibrocytes (FCs) in the spiral ligament (SL) are interconnected through gap junctions, thereby forming an outer syncytial layer. Note that tight junctions (TJs) are present in cell-cell junctions of BCs and MCs. A monolayer made of MCs is denoted as the inner layer. The circulation current flowing through the cochlear compartments is depicted. Ion channels and transporters that are critically involved in the control of electrochemical properties of the cochlea and in the maintenance of the circulation current are illustrated as well. Of note, the basolateral surface (Baso) of the syncytial layer primarily consists of FC membranes. Api: apical surface, CIC: CIC-type  $Cl^-$  channel, MET: mechano-electrical transduction channel, NKCC:  $Na^+$ ,  $K^+$ ,  $2Cl^-$ -cotransporter. **D**, summarized electrochemical profile of the lateral-wall's compartments under physiological conditions. This panel shows the potential (red) and  $[K^+]$  (blue) values obtained in representative recordings in our earlier studies.  $v_{SB}$ ,  $v_{SA}$ ,  $v_{MB}$  and  $v_{MA}$  denote the membrane potentials on the basolateral and apical surfaces of the outer syncytial layer and the basolateral and apical surfaces of the inner marginal-cell layer, respectively. Reproduced and modified from Yoshida *et al.* (2016) and Nin *et al.* (2016). [Colour figure can be viewed at [wileyonlinelibrary.com](http://wileyonlinelibrary.com)]

circuit (Fig. 2A) (Nin *et al.* 2012; 2017). In the closed loop, a current, which is composed of  $K^+$  as a net charge carrier, is circulated radially. This ‘circulation current’ is correlated with the  $[K^+]$  and potential dynamics within the stria vascularis. The model reasonably replicates the electrochemical data measured when strial channels or transporters are blocked pharmacologically or by anoxia. Here, we analysed the effects of acoustic stimuli on the non-excitabile tissue stria vascularis by combining a prediction by our computational model and *in vivo* measurement using microelectrodes sensitive to the  $[K^+]$  and potential. Both approaches detected rapid changes in the electrochemical properties of the IS. This result is direct evidence that the unidirectional circulation current links hair cells to the stria.

## Materials and methods

### Computational simulation

For *in silico* analysis (Fig. 2), the fibrocyte-integrated Nin–Hibino–Kurachi (fi-NHK) model developed in our earlier study was used (Nin *et al.* 2017). Accordingly, the principles of the model described in this section are excerpted from the previous articles with the original authors’ permission. This computational model replicates the cochlea’s three layers – i.e. the outer syncytial layer and inner layer associated with the stria vascularis in the lateral cochlear wall and the hair cell layer – as well as the ion transport system composed of the channels and transporters expressed in each layer (Fig. 2A). The model is designed on the basis of three principles as

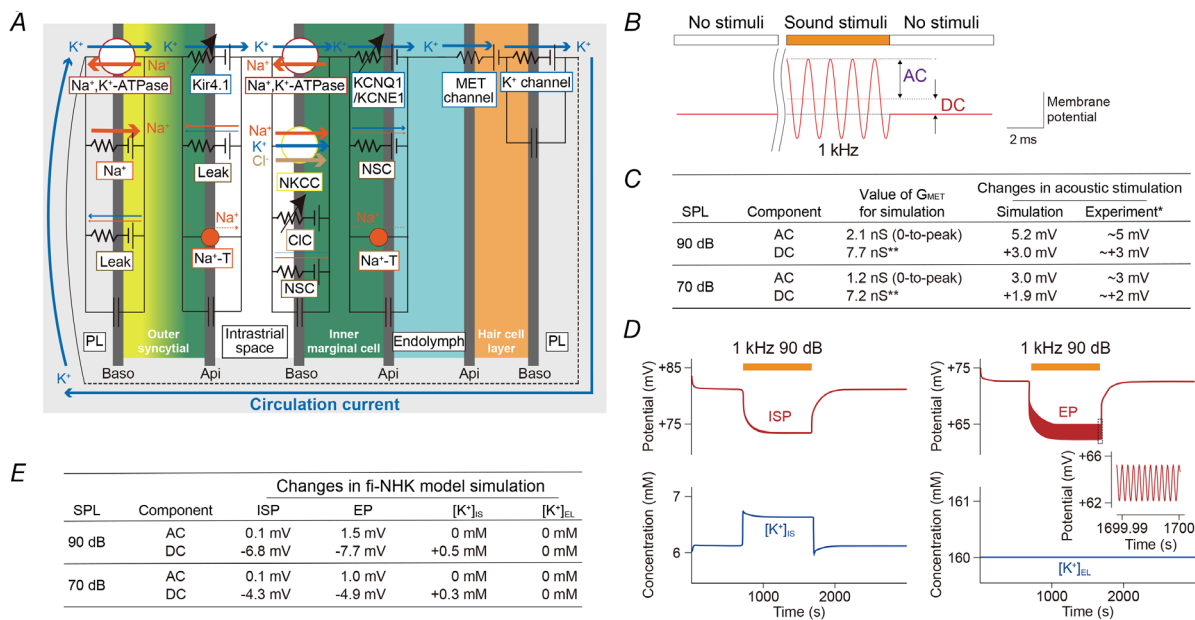


**Figure 2. Simulation of the potential and  $[K^+]$  properties in the cochlea**

A, key elements of the fi-NHK model. The scheme details all the intracellular and extracellular compartments, membrane domains and ion fluxes that are incorporated into the model. The membranes are highlighted by black bars. In the model, the outer syncytial layer, inner marginal-cell layer and hair cell layer are assembled into a series. In this arrangement, ion channels and transporters form a closed-loop circuit, which provides the pathway for the circulation current. Api: apical, Baso: basolateral, CIC: CIC-type  $Cl^-$  channel, Leak: leak conductance, MET: mechano-electrical transduction,  $Na^+$ :  $Na^+$  conductance,  $Na^+$ -T:  $Na^+$  transporter, NKCC:  $Na^+$ ,  $K^+$ ,  $2Cl^-$ -cotransporter, NSC: non-selective cation channel, PL: perilymph. B, the reproduced reaction of hair cells. The displayed schematic trace shows a change in the cellular membrane potential, which is based on *in vivo* measurements from the literature (Dallos *et al.* 1982; Dallos, 1985). In response to acoustic stimuli at 1 kHz, the potential oscillated (AC), and its middle point shifted monotonically (DC). C, parameter settings for the simulation in the mode of acoustic stimuli. To reproduce *in vivo* experimental observations of the membrane potential of an outer hair cell in a live guinea pig exposed to 1 kHz sounds at 90 and 70 dB SPL (indicated by a single asterisk (Dallos, 1985)), MET channel conductance ( $G_{MET}$ ) for the simulation was determined, as described in the panel. The displayed DC values of  $G_{MET}$  are absolute values (double asterisks); the value in a resting state was 6.4 nS. SPL: sound pressure level. D and E, electrochemical dynamics in the intrastrial space (IS) and endolymph (EL). In this analysis, the values of all the potentials and ion concentrations in the modelled cochlear compartments stabilized during 600 s after the onset of the simulation; 100 s later, the  $G_{MET}$  was configured to the conditions of 1 kHz acoustic stimuli for 1000 s, with the values determined in (C). The stimulation protocol featured neither a rising phase nor a falling phase. The traces depicted in (D) are the responses of the IS potential (ISP),  $[K^+]_{IS}$ , endocochlear potential (EP) and  $[K^+]_{EL}$  under the conditions of 90 dB stimulation. The EP data highlighted by the dotted square are longitudinally expanded in the inset panel. Steady-state values, which were obtained at the endpoint of the stimulation, are described in (E). [Colour figure can be viewed at [wileyonlinelibrary.com](http://wileyonlinelibrary.com)]

follows. Firstly, on each apical and basolateral surface in the outer syncytial layer and inner layer, ion channels and transporters, which are proven to be functional *in vivo* by electrophysiological, pharmacological and gene-targeting approaches (Wangemann, 2006; Zdebik *et al.* 2009; Fettiplace, 2017; Michalski & Petit, 2019), interact and unidirectionally transport  $K^+$  in a resting state. Secondly, these four  $K^+$  transport elements and the  $K^+$  flow across the hair cell layer are linked into a closed circuit, an arrangement that allows  $K^+$  to continuously and radially circulate between endolymph and perilymph. Thirdly, this circulation current mediated by  $K^+$  as a net charge carrier regulates the strial intra- and extracellular  $[K^+]$ -related properties that primarily determine the ISP and EP (Salt *et al.* 1987; Nin *et al.* 2008; 2012; 2017; Adachi *et al.* 2013; Yoshida *et al.* 2015; 2016).

All the formulas constituting the fi-NHK model are described in the literature (Nin *et al.* 2017) as well as in open source code (<https://doi.org/10.6084/m9.figshare.5188681.v1>). Our simulations were carried out in the MATLAB software (MathWorks, MA, USA). The key formulas of the model are as follows. Initially, the ISP and EP represent the sum of multiple membrane potentials in the stria vascularis:

$$\text{ISP} = v_{\text{SB}} - v_{\text{SA}} \quad (1)$$

and

$$\text{EP} = v_{\text{SB}} - v_{\text{SA}} + v_{\text{MB}} - v_{\text{MA}} \quad (2)$$

where  $v_{\text{SB}}$  and  $v_{\text{SA}}$  are membrane potentials across the basolateral and apical surfaces, respectively, of the outer syncytial layer, and  $v_{\text{MB}}$  and  $v_{\text{MA}}$  are those across the basolateral and apical surfaces of the inner marginal-cell layer, respectively (Fig. 2A). Each membrane potential is defined relative to the neighbouring extracellular fluid. Under normal or resting conditions, transepithelial voltage across the marginal-cell (i.e. inner) layer ( $v_{\text{MB}} - v_{\text{MA}}$ ) is small:  $<10$  mV (Salt *et al.* 1987; Nin *et al.* 2008); therefore, the EP derives primarily from the ISP.

Next, as mentioned in the principles, in the model, the circulation current is reproduced in a large closed-loop circuit, which is constructed by connecting the ion transport mechanisms of six membrane domains (i.e. the apical and basolateral surfaces of the outer syncytial layer, inner layer and hair cell layer) into a series (Fig. 2A). In this arrangement, the circulation current ( $I_{\text{Cir}}$ ) always corresponds to the current through MET channels of the hair cell layer (MET current;  $I_{\text{MET}}$ ). In accordance with the literature (Davis, 1961; Nin *et al.* 2012),  $I_{\text{Cir}}$  depends on the EP (Fig. 2A):

$$v_{\text{HA}} = -\text{EP} + v_{\text{HB}} \quad (3)$$

$$I_{\text{Cir}} = -N_{\text{HC}} \cdot I_{\text{MET}} = -N_{\text{HC}} \cdot G_{\text{MET}} \left( v_{\text{HA}} - \frac{RT}{F} \cdot \ln \left( \frac{[K^+]_{\text{EL}}}{[K^+]_{\text{HC}}} \right) \right) \quad (4)$$

where  $N_{\text{HC}}$  is the number of hair cells;  $[K^+]_{\text{EL}}$  and  $[K^+]_{\text{HC}}$  are  $[K^+]$  in endolymph and in a hair cell, respectively;  $G_{\text{MET}}$  is the conductance of MET channels;  $v_{\text{HA}}$  and  $v_{\text{HB}}$  are the membrane potentials across the hair cell apical and basolateral surfaces, respectively;  $R$  means the gas constant;  $T$  represents temperature; and  $F$  is the Faraday constant. The MET current can be detected even without acoustic stimuli ( $\sim 1$  nA per hair cell under normal conditions) (Kennedy *et al.* 2003); therefore,  $I_{\text{Cir}}$  flows through all the six membrane domains in the cochlea in a resting state.

The relationships among membrane potentials, currents across the membranes and ion concentrations of extracellular or intracellular compartments are defined as follows. Each of the six membrane potentials (see Fig. 2A) changes in accordance with the difference between the  $I_{\text{Cir}}$  that flows into a membrane and the sum of currents that move through the channels and transporters on the same membrane ( $I_{\text{M}}$ ):

$$\frac{dv}{dt} = \frac{1}{C} \cdot \frac{dQ}{dt} = \frac{I_{\text{Cir}} - I_{\text{M}}}{C} = \frac{I_{\text{Cir}} - I_{\text{K}} - I_{\text{Na}} - I_{\text{Cl}}}{C} \quad (5)$$

where  $v$  is the membrane potential,  $Q$  is the electrical charge accumulated on the membrane,  $C$  represents the capacitance of the membrane, and  $I_{\text{K}}$ ,  $I_{\text{Na}}$  and  $I_{\text{Cl}}$  denote  $K^+$ ,  $Na^+$  and  $Cl^-$  current fractions, respectively. Note that these current fractions are constituents of  $I_{\text{M}}$ . It should be emphasized again that in both the inner layer and outer layer associated with the stria,  $I_{\text{Cir}}$  is equivalent to the sum of all the currents conveyed via the channels and transporters. The other key elements are extracellular and intracellular ion concentrations. These properties can be described by means of ionic currents through the membranes:

$$\frac{d[X]}{dt} = \frac{I_{\text{X,In}} - I_{\text{X,Out}}}{V \cdot F} \quad (6)$$

where  $[X]$  is the concentration of ion X,  $I_{\text{X,In}}$  and  $I_{\text{X,Out}}$  are the inward and outward currents of X, respectively, and  $V$  is the volume of the extracellular or intracellular compartment. Because  $I_{\text{X,In}}$  and  $I_{\text{X,Out}}$  are components of  $I_{\text{M}}$  and  $I_{\text{Cir}}$ , in the steady state,  $I_{\text{Cir}}$  is equivalent to  $I_{\text{M}}$  for all membranes, and  $I_{\text{X,In}}$  is comparable to  $I_{\text{X,Out}}$  for all the compartments. This condition provides constant values for all ionic concentrations ( $d[X]/dt = 0$ ), all membrane potentials ( $dv/dt = 0$ ), and both the EP and ISP (see eqns (1) and (2)). If the currents conveyed by the channels or transporters are changed by certain perturbations, then a difference between  $I_{\text{M}}$  and  $I_{\text{Cir}}$  may arise. In such a case, the changes in the membrane potentials, ionic concentrations and EP may be simulated in the fi-NHK model.

All the parameters used for the construction and running of the model were basically the same as those in our earlier study (Nin *et al.* 2017) (open source code: <https://doi.org/10.6084/m9.figshare.5188681.v1>) and are

described in the files uploaded to figshare (see <https://doi.org/10.6084/m9.figshare.14958150> and <https://doi.org/10.6084/m9.figshare.14958153> for Tables S1 and S2, respectively). To replicate the circumstances of acoustic stimuli, as illustrated in Fig. 2B, we modulated  $G_{\text{MET}}$  sinusoidally (i.e. an AC component) and by means of a moving average (i.e. a DC component) such that the calculated membrane potential of a hair cell's basolateral surface,  $v_{\text{HB}}$ , resembled the *in vivo* measurement (see Fig. 2C) (Dallos *et al.* 1982; Dallos, 1985).

### Ethical statement and animal preparation

All the animal experiments were carried out in compliance with the protocol approved by the Institutional Animal Care and Use Committee and the President of Niigata University (Permission Number: Niigata Univ. Res. SA00407). The experiments were designed in accordance with the Japanese Animal Protection and Management Law. Male Hartley albino guinea pigs (200–350 g, 2–4 weeks of age; SLC Inc., Hamamatsu, Japan) were housed at the animal facility of Niigata University and kept on a 12 h light/12 h dark cycle. Water and food were available to the animals *ad libitum*. Animal handling and reporting complied with the ARRIVE guidelines (Kilkenny *et al.* 2010).

Guinea pigs with normal Preyer's reflex were anaesthetized adequately with an intra-peritoneal injection of 1.5 g kg<sup>-1</sup> urethane and paralysed with an intramuscular injection of 3 mg kg<sup>-1</sup> vecuronium bromide (Fuji Pharma, Tokyo, Japan). Supplemental doses of the anaesthetic were administered to ensure areflexia to the toe pinch and corneal reflex. Surgical access to the cochlea was implemented as described previously (Ogata *et al.* 2017). After tracheotomy, the guinea pigs were artificially ventilated with room air using a respirator (SN-408-7; Shinano Manufacturing, Tokyo, Japan), and their body temperature was maintained at 37°C on an isothermal pad (Deltaphase Isothermal Pad; Braintree Scientific, MA, USA). In each animal, the bulla of the left ear was surgically opened via a ventrolateral approach to expose the cochlear bony wall. The head was fixed on a head holder, and the ear was then plugged with the tip of a custom-made waveguide extending from a housed speaker (UETAX, Niigata, Japan). Then, the cochlea was subjected to the electrophysiological assays described below. After completion of the measurements, the animals were killed by urethane overdose (10 g kg<sup>-1</sup>).

### Preparation for acoustic stimuli

To detect sound-evoked changes in the auditory brainstem response (ABR), in cochlear microphonics in perilymph, and in the potential and [K<sup>+</sup>] in the IS and endolymph, sounds were generated from the speaker mentioned

above. The speaker was connected to an amplifier (RT-5; UETAX), which was controlled by the application of AC voltage between 0.1 mV and 10 V from a computer board (NI PCI-4461; National Instruments, TX, USA). Such electrical signals were produced by a computer program that we created in LabVIEW (National Instruments, TX, USA). The output port of the speaker was connected to one end of a silicone tube, which was 50 cm in length with inner and outer diameters of 0.9 and 1.4 cm, respectively. The other end of the tube was attached to a pipette tip (Gilson type 5 ml; SARSTEDT, Nümbrecht, Germany). A microphone (1/2" condenser microphone; ACO, Tokyo, Japan), which had been calibrated in advance with a sound calibrator (Type 2127; ACO), was placed at a distance of 3 mm from the edge of the tip to examine the intensity of the sound from the speaker. The protocols for acoustic stimulation in individual series of the experiments are described in the following subsections.

### Recording of cochlear microphonics

Cochlear microphonics were measured at the site of the second cochlear turn as reported elsewhere (Honrubia & Ward, 1968). In every trial, the setting of the exposed cochlea was carefully controlled under a surgical microscope such that the angle of the cochlear view was as constant as possible. On the bony wall of each cochlea, a hole of roughly 500–800  $\mu\text{m}$  was made with a microchisel at the 'central position' that was equidistant from both outline edges of the second turn (Fig. S2A). This position was visually determined under the microscope. Then, the tip of a microelectrode composed of a thin platinum wire, which was connected to an AC/DC amplifier (EX1; Dagan Corp., MN, USA), was attached to the surface of perilymph through the hole. An Ag/AgCl wire on neck muscles served as a reference. The acoustic stimulation consisted of a tone-burst sound at 50, 60 or 70 dB sound pressure level (SPL) with a 1 ms rising phase, 18 ms plateau and a 1 ms falling phase, followed by a 40 ms interval. At each sound intensity, we tested the following frequencies on five guinea pigs (Fig. 3): (1) 0.2, 0.4, 0.6, 0.8, 1.0, 1.2, 1.4, 1.6, 2.0 and 3.0 kHz for one animal (animal ID: GP089) and (2) 0.75, 1.00, 1.25, 1.50, 2.00 and 3.00 kHz for four animals (animal IDs: GP045, GP061, GP067 and GP068). Potential responses evoked by the acoustic stimuli were analysed through a bandpass filter (200–3000 Hz). The stimulation was repeated 500 times for a series of recordings. The averaged AC components were defined as cochlear microphonics. The maximum amplitude at each frequency for different SPLs was plotted to determine the tuning curve.

### Preparation of microelectrodes

Microelectrodes sensitive to the potential and [K<sup>+</sup>] were fabricated as described previously (Nin *et al.* 2008;

Adachi *et al.* 2013). The electrodes were made of double-barrelled capillary glass (World Precision Instruments (WPI); Sarasota, FL, USA). The tip diameter was less than 1  $\mu\text{m}$ . The interior of one barrel was silanized with vaporized dimethyldichlorosilane (LS-130; Shin-Etsu, Tokyo, Japan). Thereafter, the barrel was filled at the tip with a liquid ion exchanger selective for  $\text{K}^+$  (IE190; WPI) and backfilled with 150 mM KCl. The voltage barrel was filled with 150 mM NaCl. Each barrel was connected to a high-input-resistance dual electrometer (FD223a; WPI) through an Ag/AgCl electrode. The  $\text{K}^+$ -sensitive barrel was calibrated before and after each experiment, as we described before (Yoshida *et al.* 2016).  $[\text{K}^+]$  was calculated from the measured  $\text{K}^+$  activity based on an activity coefficient for  $\text{K}^+$  of 0.727 (Konishi & Salt, 1983).

### *In vivo* recording of cochlear electrochemical properties

Electrophysiological assays in the cochleae of live guinea pigs were performed by the procedure similar to that in our earlier studies (Adachi *et al.* 2013; Yoshida *et al.* 2015). Firstly, a fenestra of 200–500  $\mu\text{m}$  in diameter was made at the ‘central position’ on the bony wall of the second turn. Secondly, the double-barrelled  $\text{K}^+$ -selective microelectrode was inserted into the fenestra towards endolymph across the lateral cochlear wall using a micro-manipulator (MP-285; Sutter Instrument Co., Novato, CA, USA). The Ag/AgCl wire on the neck muscles served as a reference. At the outset of each experiment, the tip of the electrode was placed inside the perilymph, and the potential in the electrometer was adjusted to 0 mV. Therefore, throughout the experiment, the potentials were

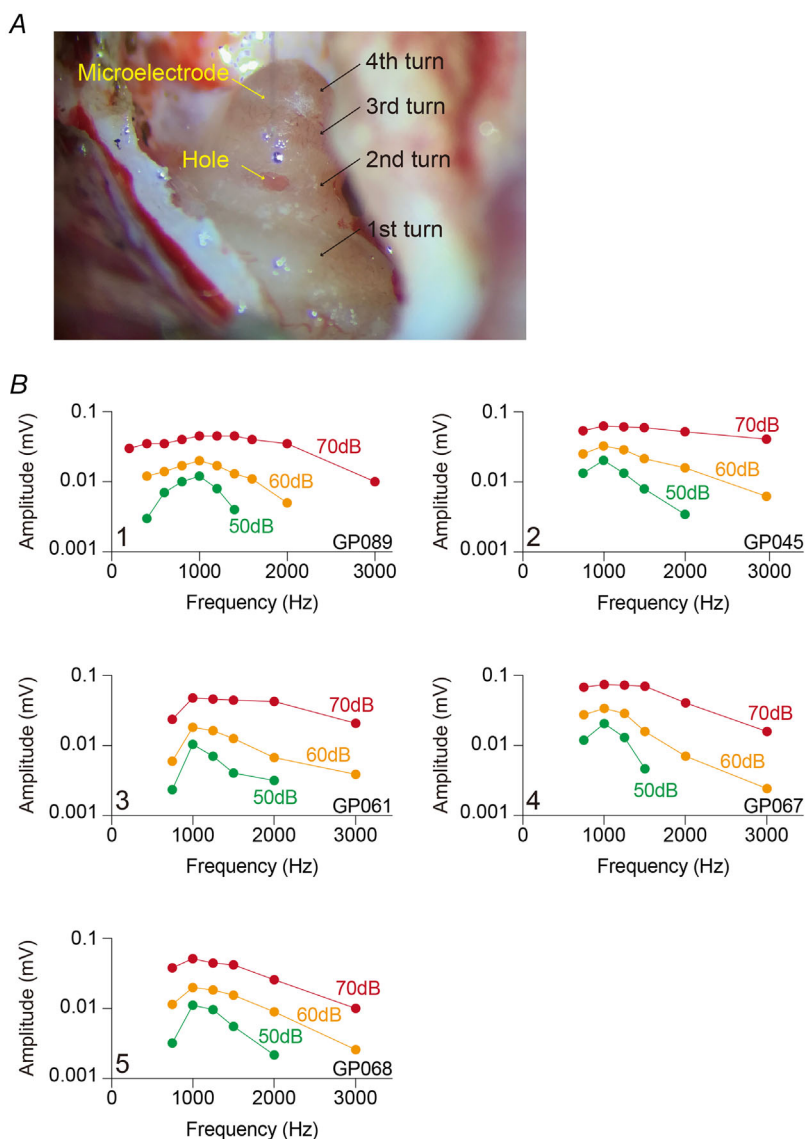


**Figure 3. Determination of the best frequency**  
 A, appearance of the cochlea in a live guinea pig. The cochlea was subjected to the surgical procedure described in the *Materials and Methods* section, and a small hole was made in a region around the centre of the cochlear second turn for insertion of an electrode, as shown in the image. Positions of the four cochlear turns are indicated. B, recording of cochlear microphonics (CM). Five guinea pigs were analysed in this series of experiments (guinea pig IDs: GP089, GP045, GP061, GP067 and GP068). In the cochlea of the left ear in each animal, CM was measured by the electrode (see A) with pure tone-burst sounds at various frequencies (200–3000 Hz) and intensities (50–70 dB sound pressure level (SPL)) (for details, see *Materials and Methods*). The acoustic stimulation consisted of a tone-burst sound at 50, 60 or 70 dB SPL with a 1 ms rising phase, 18 ms plateau and 1 ms falling phase, followed by a 40 ms interval. The amplitudes of the measured CM during each stimulation are shown in the panels. [Colour figure can be viewed at [wileyonlinelibrary.com](http://wileyonlinelibrary.com)]



measured with respect to the perilymph. During the passage of the electrode while it was inserted, the electrode was held in the IS, and the animal was exposed to a series of acoustic stimuli composed of a tone-burst sound of 1000 Hz with a 0.5 s rising phase, 9 s plateau and a 0.5 s falling phase, followed by a 30 s interval. The acoustic intensity was varied from 100 to 60 dB SPL, and the stimulation was repeated multiple times as presented in the *Results* section.

In this study, 231 guinea pigs were subjected to *in vivo* electrophysiological experiments. Among these animals, we excluded animal preparations and the resulting data if any of the following conditions were met. Firstly, when we found a deformity or effusion of the middle ear during the surgical operation, we did not proceed further (26 animals). Secondly, we discarded the data where the ISP and EP immediately before each acoustic stimulation did not exceed +70 and +80 mV, respectively (91 animals). These thresholds were determined on the basis of the averages of a number of our previous measurements with healthy cochleae (Nin *et al.* 2008; 2012; Adachi *et al.* 2013; Yoshida *et al.* 2015; 2016). In these studies, we experienced that in some guinea pigs, the EP or ISP measured under normal conditions dropped by >10 mV during stable insertion of the double-barrelled microelectrode into the IS or endolymph. This potential reduction might be owing to an increase in leakage between the IS or endolymph and the perilymph along the inserted electrode or, alternatively, owing to impairment of animal conditions. In such cases, the ISP or EP responses caused by the modulation of channels and transporters in the stria vascularis were relatively weak or insufficient. Therefore, a >10 mV drop in the ISP or EP during the measurements without acoustic stimuli was set as the third data exclusion criterion (39 animals). The following two issues stem from the literature and our prediction using these data. Acoustic stimuli at 60 dB SPL, which was the minimum intensity that we designed this study to test, reduces the EP in terms of static offset by ~0.5 mV in animal experiments (Honrubia & Ward, 1969). On such occasions, we assumed that the ISP change would not exceed the EP change, as this is the case in any previously examined conditions (Nin *et al.* 2008; 2012; Adachi *et al.* 2013; Yoshida *et al.* 2015; 2016). Therefore, fourthly, the data were discarded when noise-induced fluctuation of the ISP or EP during acoustic stimuli exceeded  $\pm 0.5$  mV (15 animals). The ISP represents the  $E_K$  on the apical surface of the outer syncytial layer (see the *Introduction* section and Fig. 1D). In this regard, with Nernst equation the ISP change of 0.5 mV in the fourth criterion corresponds to a change of  $[K^+]$  in the IS by roughly 0.2 mM when  $[K^+]$  in the syncytial layer was set to 85 mM, the typical concentration (Nin *et al.* 2008). In this context, the fifth condition was that  $[K^+]$  in the IS fluctuated by more than  $\pm 0.2$  mM (five animals). In one animal, when the electrode was advanced

in the endolymph, the  $[K^+]$  measurement became noisy and fluctuated by more than  $\pm 3$  mM, likely owing to fouling formation at the tip of the electrode during the passage across the lateral wall. We never encountered such cases in the successful experiments described in our previous works (Nin *et al.* 2008; 2012; Adachi *et al.* 2013; Yoshida *et al.* 2015; 2016); therefore, the sixth criterion was that the above-mentioned experiment was not subjected to further analysis. The seventh criterion was the drift of the perilymphatic potential and  $[K^+]$  values from the outset to the end of the recording; the former was set to  $\geq 3$  mV in accordance with the literature (Adachi *et al.* 2013). Conversion of this potential change to  $[K^+]$  change by the Nernst equation with 150 mM intracellular  $[K^+]$ , a typical physiological value in cells, provides  $\geq 5$  mM. Recordings that met these two conditions were omitted (11 animals). Eighthly, the electrode tip was broken or the shape of the tip was distorted by the insertion during the experiment; such deformation was detected by microscopic examination after *in vivo* electrochemical measurement (four animals). Ninthly, the ABR thresholds examined after the electrochemical recording exceeded 50, 45, 40, 35 and 40 dB SPL for 0.5, 1, 4, 8 and 16 kHz stimuli, respectively, the thresholds for detection of hearing loss (two animals) (Sato *et al.* 2016). Finally, 29 animals died during the experiment. Accordingly, the number of animals described in the *Results* section of the main text is eight.

### Measurement of the ABR

ABR thresholds in guinea pigs were measured as described previously (Ota *et al.* 2020). Stainless-steel needle electrodes were subcutaneously inserted into the posterior region of the neck (non-inverting) and under the pinna (inverting). Tone-burst stimuli at 0.5, 1, 4, 8 or 16 kHz were delivered to the ear. The duration of the stimulation was 3 ms, which contained a rising phase of 0.5 ms and a falling phase of 0.5 ms. For one series of the measurements, the total duration including an interval was 60 ms. Individual signals elicited from the auditory tract were amplified 5000-fold and processed with a bandpass filter (0.3–2 kHz) in an amplifier (EX-1; Dagan Corp., MN, USA). The digitized signals were averaged 1000 times (LabVIEW 2013 Service Pack 1 32-bit; National Instruments). The intensity of the acoustic stimuli was changed in 10 dB steps until a hearing threshold was determined (0 dB = 0.02 mPa).

### Statistical analysis

Means  $\pm$  SD served as descriptive statistics. Statistical significance of the data in Fig. 4 was determined with the paired *t* test (Prism 8; GraphPad Software, San Diego,

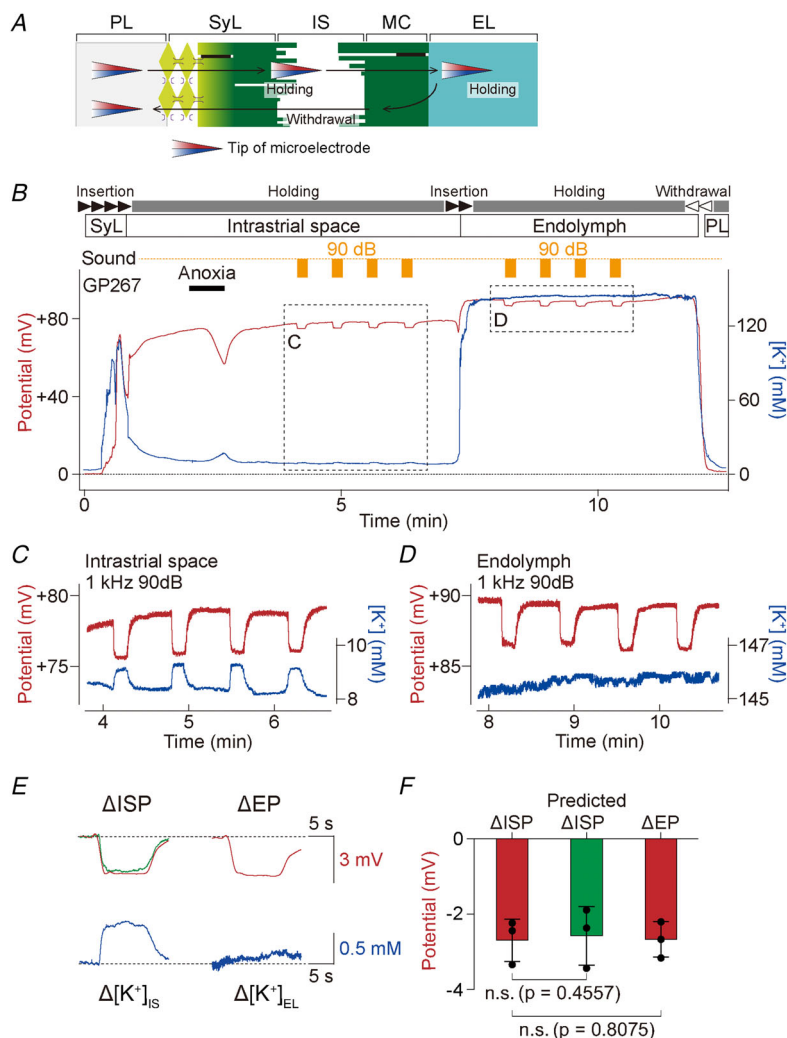


**Figure 4.** *In vivo* assays of the intrastrial space (IS) and endolymph with acoustic stimuli

A series of electrophysiological recordings in a guinea pig with a double-barrelled microelectrode sensitive to  $[K^+]$  and to the potential. As schematically illustrated in (A), the microelectrode was inserted from the perilymph to the endolymph through different compartments in the lateral cochlear wall and then pulled back to the perilymph, in which the electrode was held in the IS or endolymph. The experimental results of one animal (ID: GP267) are shown in (B). In this and subsequent recordings, the filled wedge, open wedge and grey bar above the trace denote the period when the electrode was advanced, withdrawn and held, respectively, whereas the potential and  $[K^+]$  are indicated by red and blue lines, respectively. In (B) (also see (A)), after passing through the outer syncytial layer (SyL), which was a compartment detected by means of spikes of  $[K^+]$  elevation and a low positive potential of +2.8–8.5 mV, the microelectrode was held in the IS. Imposition of anoxia on the guinea pig caused the potential to decrease and  $[K^+]$  to increase (Nin *et al.* 2008). After these parameters returned to baseline, the animal was exposed four times – at an interval of 30 s to a 1 kHz tone-burst sound, which consisted of a 0.5 s rising phase, 9 s plateau and 0.5 s falling phase, at 90 dB sound pressure level (SPL) (orange bars). Then, the electrode was inserted into endolymph (EL) and acoustic stimulation was applied to the animal by the same protocol (orange bars). The recorded responses in the IS and endolymph (dotted boxes) are expanded in (C) and (D), respectively. Panel (E) shows changes of the potential and  $[K^+]$  in the IS ( $[K^+]_{IS}$ ) and endolymph ( $[K^+]_{EL}$ ). The displayed data are ‘averaged’ traces recorded during four-time acoustic stimulation. Each trace was extracted from the recording starting from 4 s before a stimulus to 4 s after the termination of the stimulation; the data were analysed with reference to baseline. In the upper left panel of (E), the IS potential (ISP) change predicted by the Nernst equation with the measured  $[K^+]_{IS}$  increase is highlighted in green (for the formula, see the main text) and overlaid on the recorded potential change. Two other guinea pigs were also examined (#GP279 and #GP370, Fig. S1 at <https://doi.org/10.6084/m9.figshare.14958126>). In (F), individual data points as well as means  $\pm$  SD for the maximal changes in the measured ISP ( $\Delta ISP$ ), in the predicted ISP, and in the measured endocochlear potential ( $\Delta EP$ ) are displayed ( $\Delta ISP$  vs.  $\Delta EP$ ,  $n = 3$  for each,  $P = 0.8075$ ,  $t = 0.2774$ ;  $\Delta ISP$  vs. predicted  $\Delta ISP$ ,  $n = 3$  for each,  $P = 0.4557$ ,  $t = 0.9177$ ; paired  $t$  test with the Bonferroni correction for multiple comparisons). NS; not significant. [Colour figure can be viewed at [wileyonlinelibrary.com](http://wileyonlinelibrary.com)]

CA, USA). Data with a  $P$  value of  $<0.05$  were considered significant.

## Results

### The general outline of this study

The main objective of this study was to test whether the electrochemical profile of the stria vascularis is sensitive to acoustic stimuli. A key target is the behaviour of the ISP and  $[K^+]_i$ , which are the parameters associated with the EP. For this analysis, we designed two procedures: firstly, prediction of the IS response by means of our fi-NHK model (for key principles, see the *Materials and Methods* section and Nin *et al.* 2017), and secondly, verification of the simulated observations by electrophysiological experiments in live animals with microelectrodes sensitive to the potential and  $[K^+]_i$ . From the standpoint of this experimental approach, it is difficult to assess the IS by means of microelectrodes because this space is fragile and extremely narrow,  $\sim 15$  nm in width (Hinojosa & Rodriguez-Echandia, 1966). Nonetheless, we anticipated that the *in vivo* recording would continue for 10–20 min. For such a considerably prolonged experiment, we planned to focus on the centre of the second cochlear turn. This site is most stably accessible to the microelectrode and is likely characterized by approximately 1 kHz best frequency (BF), which evokes a maximal response in the threshold tuning curve (Fernandez, 1952; Honrubia & Ward, 1968). Accordingly, in the following *in silico* assay, we selected 1 kHz as the stimulus frequency.

### *In silico* analysis of effects of hair cell excitation on IS electrochemical properties

As presented in Fig. 2, we examined the effects of 1 kHz acoustic stimuli on the stria vascularis in the lateral cochlear wall via the fi-NHK model. To reproduce the hair cell response, we attempted to modulate the conductance of MET channels ( $G_{MET}$ ). To determine this parameter, we employed the electrophysiological property recorded on the soma of an outer hair cell in a live guinea pig (Dallos, 1985) (Fig. 2C) because the MET current cannot be directly measured *in vivo*. The membrane potential of the hair cell is hyperpolarized at  $-71.0$  mV in a resting state. Similar to this measurement, the steady-state value simulated under normal conditions (i.e. without any stimuli) was  $-77.7$  mV when  $G_{MET}$  was set to 6.4 nS (Hudspeth, 1989; Nin *et al.* 2012; 2017). Classic *in vivo* recordings suggest that pure tone-burst acoustic stimuli at 1 kHz oscillate the hair cell potential at the same frequency and produce a static offset depolarization (Dallos *et al.*

1982; Dallos, 1985), as shown in Fig. 2B. In the literature, the measured offset magnitude and oscillation amplitude at 90 dB SPL are approximately  $+3$  and 5 mV, respectively, in a steady state. Such DC and AC responses diminish to approximately  $+2$  and 3 mV, respectively, when the stimulus intensity is reduced to 70 dB SPL. These hair cell-related measurements were reasonably replicated by the fi-NHK model when the DC and AC parameters of  $G_{MET}$  were set to 7.7 and 2.1 nS (0-to-peak) for 90 dB SPL and to 7.2 and 1.2 nS (0-to-peak) for 70 dB SPL (Fig. 2C).

Figure 2D illustrates the simulated dynamics of the electrochemical properties of the IS and endolymph. Under normal conditions (i.e. in a resting state;  $G_{MET} = 6.4$  nS), steady-state values of the ISP and  $[K^+]_i$  in the IS ( $[K^+]_{IS}$ ) were  $+81.1$  mV and 6.1 mM, respectively; additionally, those of the EP and  $[K^+]_i$  in endolymph ( $[K^+]_{EL}$ ) were  $+72.2$  mV and 160 mM, respectively. These values are consistent with the actual measurements (Nin *et al.* 2008). Then,  $G_{MET}$  parameters were configured for the mode of 1 kHz acoustic stimuli at 90 dB SPL for 1000 s (see also Fig. 2C). As soon as this perturbation began, the ISP immediately dropped by 3.7 mV in terms of its static offset. The potential continuously diminished and reached a plateau at  $\sim +74.5$  mV in 400 s. The time constant of this DC change was 46 s. Only minimal oscillation of the potential was detected. The ISP returned to the initial level in 900 s when the  $G_{MET}$  parameters were switched back to the values corresponding to normal conditions. We observed a static offset response of  $[K^+]_{IS}$  with no AC component. Careful examination revealed that the configuration of acoustic stimuli resulted in a rapid increase in  $[K^+]_{IS}$  by 0.7 mM, followed by a modest recovery by  $\sim 0.1$  mM. The value stabilized at  $\sim 6.6$  mM in 400 s from the outset of the stimulation. Upon cessation of this perturbation,  $[K^+]_{IS}$  immediately recovered and manifested a slight undershoot before returning to the initial level. Furthermore, electrochemical properties of endolymph were assayed in detail (Fig. 2D). In this compartment, the potential (i.e. EP) during the acoustic stimulation mode (90 dB SPL) showed behaviour similar to that of the ISP, except for the AC component. At the outset of the stimuli, the DC component of the EP diminished by 7.7 mV at most with a time constant of 46 s, as observed in the ISP change. This static offset was accompanied by clear oscillations; the amplitude in a steady state was 1.5 mV. The AC value greatly exceeded the amplitude of the ISP (0.1 mV). Neither DC nor AC changes were detectable in  $[K^+]_{EL}$ . When 70 dB SPL stimulation was tested in the model (for  $G_{MET}$  values, see Fig. 2C), the reactions of the potential and  $[K^+]_i$  in the IS and EP moderately weakened as compared with the case of 90 dB SPL (Fig. 2E), suggesting that these values depend upon stimulus intensity.

### **In vivo measurements of the IS electrochemical properties with acoustic stimuli**

The fi-NHK model indicated that sounds can induce small but significant changes in the electrochemical properties of the stria vascularis (Fig. 2). We next verified this supposition by an *in vivo* experiment with acoustic stimuli at 1 kHz. As for the double-barrelled microelectrode we used, the measured resistance and capacitance of the tip sensitive to the potential were  $\sim 50\text{ M}\Omega$  and  $\sim 16\text{ pF}$ , respectively, yielding a cut-off frequency of  $\sim 200\text{ Hz}$ . Owing to this limitation, the electrode is unlikely to record AC reactions at 1 kHz. Accordingly, we focused upon the static offset, i.e. DC responses, in the following assays.

As experimental animals, we chose guinea pigs because they have been previously used for assays of the membrane potential in outer hair cells (Dallos *et al.* 1982; Dallos, 1985). Each site along the cochlear spiral is highly tuned in terms of frequency; the basal region is sensitive to high-pitch sounds, whereas the apex is excited by low-frequency stimuli (Fernandez, 1952; Honrubia & Ward, 1968). The second cochlear turn responds to the frequencies of 0.5 to 2 kHz (Fernandez, 1952; Békésy & Wever, 1960). For electrophysiological experiments, we targeted a region around the centre of the second turn in individual guinea pigs (Fig. 3A), for the reason mentioned in *The general outline of this study* (see also *Materials and Methods*). Initially, we determined whether the BF in the target region was 1 kHz. For this purpose, we measured cochlear microphonics, which represent the activity of hair cells, in perilymph while exposing an animal to pure tone-burst sounds at various frequencies (200–3000 Hz) and intensities (50–70 dB SPL). When the applied sound pressure was 50 dB, AC amplitude of the cochlear microphonics peaked at 1 kHz in all five animals examined (Fig. 3B). This observation is similar to that reported in the literature (Honrubia & Ward, 1968). Overall, in the target portion, 1 kHz is likely to be the BF or close to it in our experimental preparations.

For electrochemical analysis, we first stimulated anaesthetised guinea pigs with a sound at a constant pressure level of 90 dB. During the recording, the double-barrelled microelectrode sensitive to the potential and  $[\text{K}^+]$  was advanced or held in individual compartments of the lateral cochlear wall, as described in Fig. 4A. Figure 4B–4D illustrates representative measurements. The microelectrode was inserted into the perilymph of the target region and was pushed towards endolymph through the lateral wall (Fig. 4B). At the outset, the microelectrode in perilymph recorded a  $[\text{K}^+]$  of 5.1 mM. Upon the advance of the electrode, we noticed fluctuations of the  $[\text{K}^+]$  and potential; their peak values, respectively, ranged from 26.5 to 92.7 mM and from +2.8 to +11.5 mV. These data are consistent with the profile of the outer syncytial layer composed of numerous

cells (Fig. 1C) (Nin *et al.* 2008). When inserted further, the microelectrode encountered the IS that featured a low  $[\text{K}^+]$  of 8.6 mM and a high potential of +78.2 mV (Fig. 4B) (Adachi *et al.* 2013; Yoshida *et al.* 2015; 2016). While holding the double-barrelled microelectrode in this extracellular compartment, we imposed anoxia on the guinea pig for a short period. This perturbation slowly but markedly decreased the potential and increased  $[\text{K}^+]$ : a typical response for the IS (Nin *et al.* 2008; 2016; Yoshida *et al.* 2015; 2016). After the two parameters returned to baseline under normoxia, we exposed the animal to four sequential stimulation pulses, each of which was composed of tone-burst sounds lasting 10 s (Fig. 4B and C; for the stimulation protocol, see *Materials and Methods*). The ISP responded to all the pulses in a similar manner. In addition, roughly symmetrical reactions of  $[\text{K}^+]_{\text{IS}}$  were observed. To analyse the kinetics of the responses, we extracted the traces of the recorded potential and  $[\text{K}^+]$  for 18 s starting from the time point of 4 s before each stimulation pulse, and then we averaged the four sets of data with reference to baseline in each case. In the averaged traces (Fig. 4E), the acoustic stimulation abruptly caused the potential to decrease by 2.7 mV and  $[\text{K}^+]$  to increase by 0.74 mM; the time constant ( $\tau$ ) of the former was similar to that of the latter ( $\sim 0.8\text{ s}$ ). After reaching peak values, the responses were relatively stable. Upon cessation of the stimulation, both the potential and  $[\text{K}^+]$  returned to baseline levels in 2 s. As displayed in Fig. 4B, in the resting state, the microelectrode was inserted further into endolymph, which manifested a highly positive potential of +89.3 mV and a high  $[\text{K}^+]$  of 145.8 mM (Nin *et al.* 2008). Subsequently, the same stimulation protocol as that used for the IS analysis was applied to the animal. As observed for the ISP (see Fig. 4B), in response to each pulse, the EP decreased in terms of its static offset (Fig. 4D). In the averaged trace (Fig. 4E), the maximal amplitude and time constant of the change were 2.5 mV and 0.8 s, respectively. This profile, which is similar to the data in the literature (Honrubia & Ward, 1969), is quantitatively comparable to the profile obtained for the ISP. In contrast,  $[\text{K}^+]_{\text{EL}}$  was changed only minimally by each pulse stimulation (Fig. 4B, 4D and 4E) (Salt & Konishi, 1979). As expected from the cut-off frequency of the electrode, the AC component was barely detectable throughout the measurement. Overall, the electrochemical measurements described above matched the results of the simulation via the fi-NHK model (see Fig. 2).

Next, we determined whether and how the behaviour of the ISP during the acoustic stimuli was related to that of  $[\text{K}^+]$  inside the IS. The ISP is defined by eqn (1) (Nin *et al.* 2008; 2012), where  $v_{\text{SB}}$  and  $v_{\text{SA}}$  are membrane potentials across the basolateral and apical surfaces of the outer syncytial layer, respectively (Fig. 1C and Fig. 2A). *In vitro* and *in vivo* electrophysiological experiments have

previously revealed that  $v_{SA}$  is mostly determined by  $E_K$  (Takeuchi *et al.* 2000; Nin *et al.* 2008). Therefore, the ISP (Nin *et al.* 2012) can be described as

$$ISP = v_{SB} - v_{SA} \approx v_{SB} - \frac{RT}{F} \ln \left( \frac{[K^+]_{IS}}{[K^+]_{SY}} \right) \quad (7)$$

where  $[K^+]_{IS}$  and  $[K^+]_{SY}$  denote  $[K^+]$  respectively inside the IS and outer syncytial layer,  $R$  means the gas constant,  $T$  represents temperature, and  $F$  is the Faraday constant. Fibrocytes in the spiral ligament, which constitute the majority of the basolateral surface of the outer syncytial layer (Fig. 1C), have thin and infolded processes and a small quantity of cytoplasm (Kikuchi *et al.* 1995; Spicer & Schulte, 1996). Because of these characteristics, it is technically difficult to hold the electrode inside the fibrocytes and monitor the membrane potential,  $v_{SB}$ , and  $[K^+]_{SY}$  as a function of time (Adachi *et al.* 2013; Yoshida *et al.* 2016). Therefore, we assumed that these two parameters would be constant during acoustic stimuli. In this case, the change in the ISP ( $\Delta ISP$ ) can be represented by that of  $[K^+]_{IS}$ :

$$\Delta ISP \approx \Delta \frac{RT}{F} \ln ([K^+]_{IS}) \quad (8)$$

As depicted in Fig. 4E, we calculated  $\Delta ISP$  dynamics via eqn (8) from the averaged changes in the  $[K^+]_{IS}$  trace induced by the four pulses; at any time points, the prediction closely corresponded to the amplitude of the measured ISP reduction. Similar results were obtained in two other guinea pigs, although the recorded ISP and  $[K^+]_{IS}$  changes varied to some extent among the individuals (Fig. 4F;  $2.7 \pm 0.6$  mV for  $\Delta ISP$  and  $2.6 \pm 0.8$  mV for predicted  $\Delta ISP$ ; mean  $\pm$  SD;  $n = 3$ ;  $P = 0.4557$  and  $t = 0.9177$ , determined by the paired  $t$  test with the Bonferroni correction for multiple comparisons; see also Fig. S1 in <https://doi.org/10.6084/m9.figshare.14958126> for raw data). Accordingly, the sound-induced response of the ISP can be explained primarily by the  $E_K$  change that derives from the modulation of  $[K^+]_{IS}$ .

The EP represents the sum of the transepithelial voltage across the outer syncytial layer and that across the inner layer (Nin *et al.* 2008; 2012; Adachi *et al.* 2013; Yoshida *et al.* 2015; 2016). Nevertheless, similarities between the ISP and EP changes during acoustic stimuli were observed in all three guinea pigs (Fig. 4C and 4D; Fig. S1 at <https://doi.org/10.6084/m9.figshare.14958126>). The averages of the maximal values were  $2.7 \pm 0.6$  mV for  $\Delta ISP$  and  $2.7 \pm 0.5$  mV for  $\Delta EP$  (Fig. 4F; mean  $\pm$  SD;  $n = 3$ ;  $P = 0.8075$  and  $t = 0.2774$ , determined by the paired  $t$  test with the Bonferroni correction for multiple comparisons). These observations indicated that the transepithelial voltage across the inner layer was only minimally affected by the acoustic stimuli.

## Measurement of intensity and frequency dependences of the IS properties

We next tested whether the amplitudes of potential and  $[K^+]$  changes in the IS depend upon SPL. For this purpose, we again inserted the double-barrelled microelectrode into this extracellular space in a different guinea pig and stimulated the animal with 1 kHz tone-burst sounds at various intensities (60–100 dB SPL in 10 dB steps; Fig. 5A) (for the stimulation protocol, see *Materials and Methods*). The stimulation at each intensity was composed of four repeated pulses, as illustrated in Fig. 4. According to the experimental results shown in Fig. 5A–5C, the responses of the ISP and  $[K^+]_{IS}$  were likely to diminish as the sound intensity was decreased. This tendency was clearer after the averaging of traces in the data from the four pulses (Fig. 5D). Similar results were observed in the other two guinea pigs, although, again, the amplitudes of the potential and  $[K^+]$  changes varied among the individuals to some extent (Fig. 5E; see Fig. S1 at <https://doi.org/10.6084/m9.figshare.14958126> for raw data). It is also notable that the ISP reduction calculated via eqn (3) with the measured  $[K^+]_{IS}$  change was similar to the recorded ISP changes at any sound pressure (Fig. 5E).

Finally, in the experiment presented in Fig. 6A, a guinea pig was exposed to acoustic pulses of 70 dB SPL at various frequencies (0.50, 0.75, 1.00, 1.25, 1.50, 2.00, 2.50, 3.00 and 4.00 kHz, 10 s for each pulse). Before the IS analysis, we confirmed that during the application of the 1 kHz sound at 100 dB SPL, the electrode placed in perilymph detected little change in the potential and  $[K^+]$ . In the IS, the responses of the potential and  $[K^+]$  were symmetrical and considerably tuned in terms of the frequency. Among the different frequencies at the constant SPL of 70 dB, the greatest change in both metrics was detected at 1 kHz, which was the BF in the target portion (see Fig. 3). The reaction decayed as the frequency was deviated far from the BF (Fig. 6B and 6C). With acoustic stimuli of 70 dB SPL,  $Q_{3dB}$  for the ISP (3.64) was comparable to that for  $[K^+]_{IS}$  (3.85). This result indicates a close correlation between the two parameters. When a different guinea pig was tested with stimuli of 90 dB SPL, the recorded tuning curves were broader (Fig. 6C; for raw data, see Fig. S2 at <https://doi.org/10.6084/m9.figshare.14958141>);  $Q_{3dB}$  values for the ISP and  $[K^+]_{IS}$  were 1.18 and 1.33, respectively. Thus, the electrochemical modulation of the IS depends on the frequency.

## Discussion

In this study, we analysed the stria vascularis in the 1 kHz BF region and found that the strial electrochemical properties are sensitive to acoustic stimuli. Initially, the fi-NHK model showed that the configuration mimicking the stimulation caused the ISP to decrease

and  $[K^+]_{IS}$  to increase (Fig. 2). These responses were reversible. The predicted DC changes semi-quantitatively matched the results of the *in vivo* experiment (Fig. 4 and Fig. S1 at <https://doi.org/10.6084/m9.figshare.14958126>). The recorded static offset of the ISP was small ( $\Delta ISP = 2.7 \pm 0.6$  mV at 90 dB SPL,  $n = 3$ ; Fig. 4F). Nevertheless, this measurement result seems to make sense because the amplitude is comparable not only to the

DC component of the hair cell depolarization ( $\sim 3.0$  mV at 90 dB SPL) but also to the DC shift of cochlear microphonics detected in the scala tympani and scala media ( $\sim 3.5$  mV for each at 90 dB SPL) (Honrubia & Ward, 1968; Dallos, 1985). Similarly, the EP's static offset that we noted was modest ( $\Delta EP = 2.7 \pm 0.5$  mV at 90 dB SPL;  $n = 3$ ; Fig. 4F) (Honrubia & Ward, 1969). Moreover, we identified intensity and frequency dependences of the

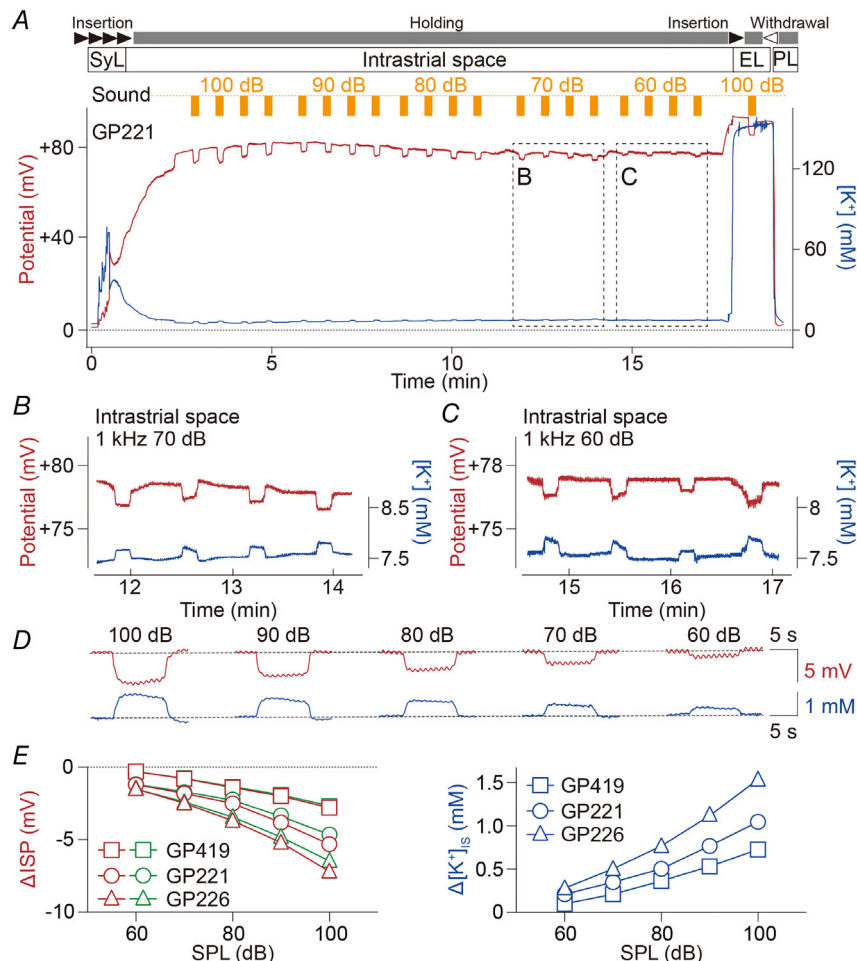


### Figure 5. Relationship between the properties of the intrastrial space (IS) and intensity of acoustic stimuli

In this recording, the double-barrelled microelectrode was pushed from perilymph to endolymph (EL) to measure the potential (red) and  $[K^+]$  (blue) in the cochlea of a live guinea pig (animal ID: GP221). As indicated in panel (A), after passing through the outer syncytial layer (SyL), the electrode tip was placed in the intrastrial space (IS). The guinea pig was exposed to the 1 kHz tone-burst sound four times with an interval of 30 s at each intensity (100 to 60 dB SPL, 10 dB step; orange bars). The stimulation protocol was the same as that used in Fig. 4. Thereafter, the electrode was advanced into endolymph (EL), which showed a high potential similar to the ISP and a high  $[K^+]$  of 145.3 mM in a resting state. In this compartment, the response was recorded with a single 100 dB SPL stimulus. Finally, the electrode was pulled back to perilymph, confirming the negligible drift of the potential and  $[K^+]$ . The measured electrochemical responses in the IS at 70 and 60 dB SPL (dotted boxes) are enlarged in (B) and (C), respectively. D illustrates the averaged traces of the potential and  $[K^+]$  changes induced during each of the five series of acoustic stimulation procedures (100–60 dB SPL). The analyses were the same as those used in Fig. 4E. Two other guinea pigs (#GP226 and #GP419) were examined by the same experimental procedure (Fig. S2 at <https://doi.org/10.6084/m9.figshare.14958141>); in panel (E), the maximal values of the averaged potential and  $[K^+]$  changes in the IS for three animals are plotted as a function of acoustic intensity. [Colour figure can be viewed at [wileyonlinelibrary.com](http://wileyonlinelibrary.com)]

ISP and  $[K^+]$  (Figs 5 and 6; Figs S2 and S3 at <https://doi.org/10.6084/m9.figshare.14958141> and <https://doi.org/10.6084/m9.figshare.14958144>, respectively).

**Evidence for electrical coupling of hair cells to the stria vascularis by the circulation current**

It has been suggested that the sound-induced reduction in the EP is simply due to an increased leakage current between the endolymph and perilymph in response to a reduction in hair cell resistance (Davis, 1957; Davis *et al.* 1958). This assumption excludes the involvement of the stria vascularis so that it cannot account for our experimental observations in the IS (Figs 2 and 4–6). Nonetheless, the relationship between the stria and hair cells is described in a few other conventional theories. In the first theory, the electrical profile of the hair cell is represented by variable resistance and a battery, and these cellular elements are connected serially to the battery in the stria vascularis (Davis, 1953; 1958; 1965) (see *Introduction*). In this closed or local circuit, the radial standing current can flow even under resting conditions; acoustic stimuli can magnify the current by reducing hair cell resistance. Later, researchers have proposed that energy status of the strial battery depends simply and solely upon its own aerobic metabolism, but they have not discussed

the relevance of hair cell activity to battery components (Thalman *et al.* 1972; Wada *et al.* 1979). The second hypothesis, known as ‘ $K^+$  recycling’ theory, postulates that  $K^+$  is transported unidirectionally and continuously through a pathway composed of at least hair cells, the stria vascularis, and spiral ligament, and this phenomenon may compensate sound-induced loss of  $K^+$  from endolymph (Kikuchi *et al.* 1995; 2000a; Spicer & Schulte, 1996; 1998; Weber *et al.* 2001; Wangemann, 2002; 2006). Moreover, the  $K^+$  recycling is assumed to ensure  $[K^+]_{IS}$  homeostasis crucial for the ISP in conjunction with a so-called ‘two-cell model’ or ‘five-compartment model’, which proposes the EP as the sum of two transepithelial voltages in the strial outer layer and inner layer (Salt *et al.* 1987; Takeuchi *et al.* 2000; Wangemann, 2006). These models, however, specify neither an electrical loop circuit nor a radial standing current for the cochlea. In other words, none of the concepts mentioned above can help to determine the mechanism by which the strial electrochemical properties respond almost in ‘real time’ to the modulation of hair cell activity by acoustic stimuli. The only solution to this enigma seems to be our fi-NHK model, which combines Davis’s theory,  $K^+$  recycling theory, and the five-compartment model and additionally makes provisions for reciprocal interplay between the circulation current and strial  $[K^+]$  and potential dynamics

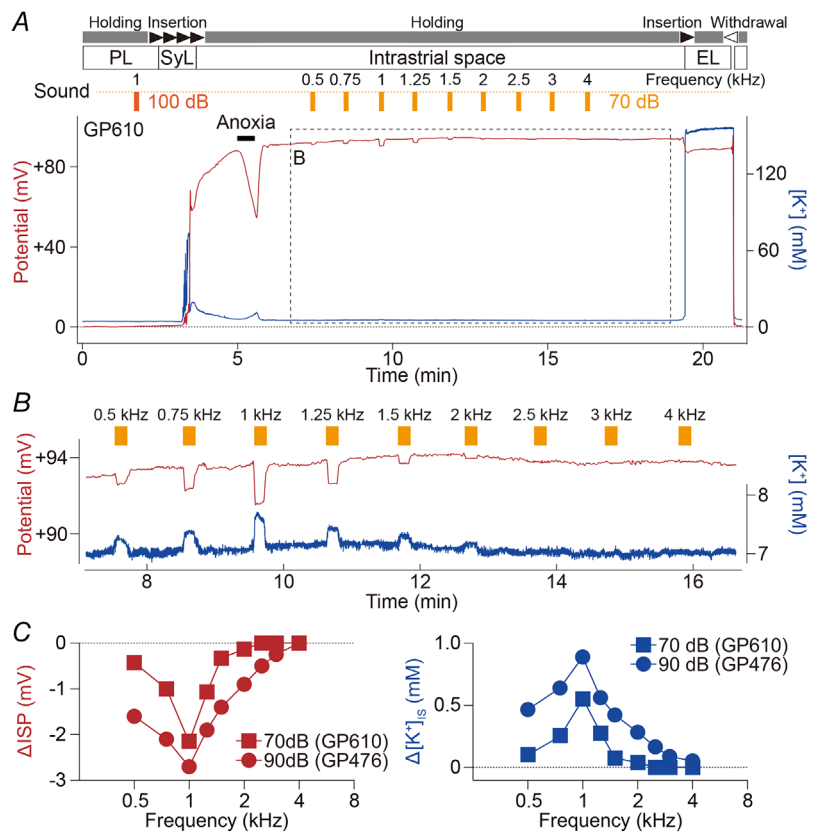


**Figure 6. The tuning curve of the potential and  $[K^+]$  in the intrastrial space (IS)**  
 In this experiment (A), initially, 1 kHz tone-burst stimulation (a 0.5 s rising phase, 9 s plateau and 0.5 s falling phase) at 100 dB sound pressure level (SPL) was applied to a live guinea pig (animal ID: GP610) while the double-barrelled microelectrode was placed in perilymph. Then, the microelectrode was held in the IS and 70 dB tone-burst stimuli at frequencies of 0.50, 0.75, 1.00, 1.25, 1.50, 2.00, 2.50, 3.00 and 4.00 kHz (each interval: 50 s) were sequentially administered to the animal. The stimulation protocol was the same as that utilized in Fig. 4. The measured potential and  $[K^+]$  are highlighted in red and blue, respectively. Anoxia was applied to confirm electrode location in the IS. The responses detected after the acoustic stimuli (boxed regions) are enlarged in (B). In this context, the highest values of the potential and  $[K^+]$  changes are plotted as a function of stimulus frequency in (C). This panel additionally presents the measurement with a series of 90 dB stimuli in a different animal (#GP476) (Fig. S3 at <https://doi.org/10.6084/m9.figshare.14958144>). [Colour figure can be viewed at [wileyonlinelibrary.com](http://wileyonlinelibrary.com)]

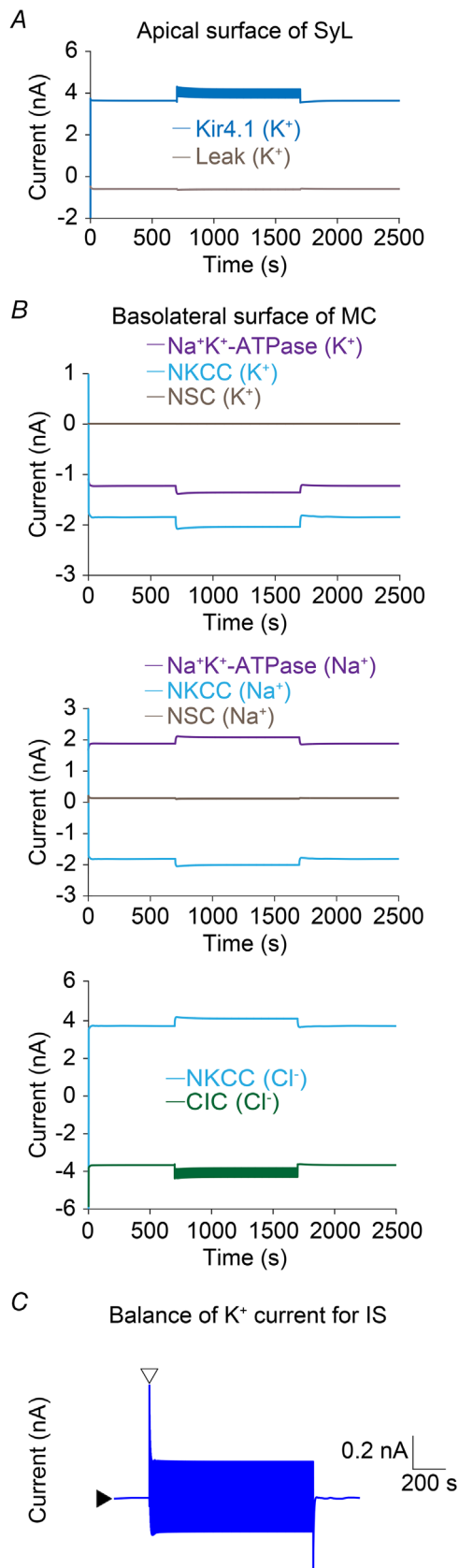


**Figure 7.** Simulated currents for the ion channels and transporters associated with the intrastrial space (IS)

From the simulation result described in Fig. 2D, each ionic current carried by ion transport mechanisms on the apical surface of the outer syncytial layer (SyL) and basolateral surface of the inner marginal-cell layer (MC) was extracted and shown in panels (A) and (B), respectively. The conditions of 1 kHz acoustic stimuli were provided for the fi-NHK model at the timepoint of 700 s from the outset of the calculation and maintained for 1000 s. The names of the channels and transporters, whose localization in the stria vascularis is illustrated in Fig. 2A, and the types of ion currents are displayed in each panel. Outward current was defined as positive. Note that a significant AC response was observed in the K<sup>+</sup> current via Kir4.1 and Cl<sup>-</sup> currents in CIC-type Cl<sup>-</sup> channels (CIC) (bold traces in (A) and (B), respectively). In (C), the balance between the total K<sup>+</sup> outflow from the IS (i.e. the sum of K<sup>+</sup> currents via K<sup>+</sup> transport mechanisms on the basolateral surface of MC (B) and the total inflow into the IS (i.e. the sum of K<sup>+</sup> currents via K<sup>+</sup> transport mechanisms on the apical surface of SyL (A) was calculated and displayed. We observed a transient increase in the K<sup>+</sup> inflow at the outset of the acoustic stimulation (open arrowhead), followed by a stabilized AC response, whose centre value matched the baseline level detected without acoustic stimuli (filled arrowhead). Leak: leak conductance, NKCC: Na<sup>+</sup>,K<sup>+</sup>,2,Cl<sup>-</sup>-cotransporter, NSC: non-selective cation channel. [Colour figure can be viewed at [wileyonlinelibrary.com](http://wileyonlinelibrary.com)]

on the basis of measurements within the stria (Fig. 2A) (Nin *et al.* 2012; 2017). In turn, the similarity between the simulated results and experimental observations in this study indicates that *in vivo*, the circulation current, which is equivalent to the radial standing current (Zidanic & Brownell, 1990), exists, and the current indeed electrically and serially couples the stria vascularis to hair cells, as suggested previously (Davis, 1953; 1958; 1965; Nin *et al.* 2012; 2017). Similarly to an idling current, the circulation current is likely to permit hair cells to respond immediately to mechanical stimuli as well as to ensure electrochemical homeostasis within the cochlea (Davis, 1961; Zidanic & Brownell, 1990; Patuzzi, 2011). Our work indicates that this physiologically relevant current is maintained by the cochlear 'system', which results from a network of K<sup>+</sup> transport mechanisms in the stria and hair cells.

The processes behind the observed ISP and EP changes can be mostly explained as follows. The circulation current, which flows across the stria vascularis as well, is modulated by a sound-induced change in the MET current. This step should modify the currents through the strial channels and transporters, thereby leading to an increase in [K<sup>+</sup>]<sub>IS</sub>, which primarily underlies the ISP and EP (Figs 4E, 4F and 5D). To support this idea, from the results of the simulation with the fi-NHK model, we extracted each ionic current carried by individual channels and transporters on the membrane domains facing the IS (Fig. 7). Acoustic stimuli changed the currents not only through the Kir4.1 K<sup>+</sup> channel on the apical surface of the outer syncytial layer (Fig. 7A) but also through ion transport mechanisms on the basolateral surface of the inner marginal-cell layer (Fig. 7B).



When analysing the balance between the total  $K^+$  outflow from the IS and the total inflow to the IS, we found a transient increase in the latter at the outset of the stimulation (Fig. 7C). This phenomenon could result in a sound-induced increase in  $[K^+]_{IS}$ . Thereafter, the balance immediately returned to the baseline (Fig. 7C), which mirrors the steady state of  $[K^+]_{IS}$  during the stimulation (see Fig. 2D). Additionally, in the AC change, the increase and decrease of the  $K^+$  current balance for the IS are symmetrical (Fig. 7C); therefore, net  $[K^+]_{IS}$  is not affected. It must be emphasized that these observations were obtained from the simulation; therefore, further studies will be necessary to prove the proposed mechanisms.

Notably, in our *in vivo* experiments, acoustic stimuli negligibly affected endolymphatic  $[K^+]$  (Figs 4B and 5A), regardless of possible changes in the amplitude of the circulation current. This result is likely due to the relatively large volume of the endolymphatic space, that is, the scala media.

A disturbance of the circulation current may be involved in the phenotypes of animal models of acoustic trauma. Exposure of the ear to loud sounds causes damage to not only hair cells but also the stria vascularis (Robertson & Johnstone, 1980; Hirose & Liberman, 2003). As a consequence, strial cells become abnormally swollen and eventually degrade (Wang *et al.* 2002). This pathological phenomenon seems to be due to impaired homeostasis of the ionic milieu within the stria. In this context, it is reasonable to hypothesize that the ionic imbalance is induced by excess modification of the circulation current. Conversely, circulation current regulation by the modification of the ion transport mechanisms in the stria may prevent hair cells from being damaged by loud sounds. Indeed, administration of furosemide, an  $Na^+, K^+, 2Cl^-$ -cotransporter blocker, before noise exposure, can protect the cochlea from acoustic trauma in mice (Adelman *et al.* 2010). This transporter, which is expressed on the basolateral surface of the inner marginal-cell layer and critically contributes to the circulation current (Figs 1C and 2A), may be a target for an advanced therapeutic intervention that protects hair cells.

### The difference in frequency dependence between IS's responses and the membrane potential of hair cells

$Q_{3dB}$  at 70 dB SPL, a sharpness index for the frequency dependence, for the ISP and  $[K^+]_{IS}$  (3.64 and 3.85, respectively; Fig. 6) was less than the value obtained from the tuning curve of the membrane potential of outer hair cells ( $\sim 5.3$ ) (Dallos *et al.* 1982). This discrepancy may be explained as follows. *In vivo*, individual hair cells are separated by tight junctions (Ben-Yosef *et al.* 2003); thus, they are likely to be electrically isolated. From this standpoint, it is necessary to consider the situation

where the hair cell tuning curve is determined by the insertion of a microelectrode into a single cell (Dallos *et al.* 1982; Dallos, 1985). In contrast, the invaginated IS is anatomically extended and must be connected from the base to apex along the cochlea axis. Therefore, in the IS, the parameters at the measurement point of the 1 kHz BF may be affected by the electrochemical changes induced in the neighbouring regions to some extent. This contamination could explain, at least in part, the broadening of the tuning curve of the strial response (Fig. 5C), as compared with the hair cell.

### Limitations of this study

The amplitudes of sound-induced DC responses of IS properties and EP in the simulation were qualitatively similar to – but not perfectly consistent with – the values obtained in the experiments (Figs 2E, 4F and 5E). In addition, the time constants for the changes in the ISP and  $[K^+]_{IS}$  significantly exceeded the measured values (Figs 2D, 4F and 5D). These discrepancies may be due to the following limitation: some of the parameters utilized in our model were derived from the *in vitro* data on cell samples isolated from the stria vascularis. Further revision and fine-tuning of the fi-NHK model will be necessary for more accurate simulations. Moreover, careful examination of each measurement in Figs 4E and 5E revealed that the sound-induced DC change of the ISP was slightly larger than the  $E_K$  shift calculated from the measured change of  $[K^+]_{IS}$  by means of the Nernst equation, although no significant difference in the data between these two groups was detected by statistical analysis. In this  $E_K$  calculation, we hypothesized that  $v_{SB}$  and  $[K^+]_{SY}$  are constant, even during acoustic stimuli. This might not be the case for live guinea pigs. Another possibility is related to the circulation current. Constant flow of this current in the closed cochlear circuit may cause slight voltage drops when it goes through the resistance in the ion channels on each membrane domain. Aside from the  $E_K$  change, such a component must be included in the reduction of the ISP. In electrical engineering, this scenario is reminiscent of the voltage drop resulting from internal resistance within a battery integrated into a closed circuit.

### References

- Adachi N, Yoshida T, Nin F, Ogata G, Yamaguchi S, Suzuki T, Komune S, Hisa Y, Hibino H & Kurachi Y (2013). The mechanism underlying maintenance of the endocochlear potential by the  $K^+$  transport system in fibrocytes of the inner ear. *J Physiol* **591**, 4459–4472.
- Adelman C, Perez R, Nazarian Y, Freeman S, Weinberger J & Sohmer H (2010). Furosemide administered before noise exposure can protect the ear. *Ann Otol Rhinol Laryngol* **119**, 342–349.

- Ando M & Takeuchi S (1999). Immunological identification of an inward rectifier K<sup>+</sup> channel (Kir4.1) in the intermediate cell (melanocyte) of the cochlear stria vascularis of gerbils and rats. *Cell Tissue Res* **298**, 179–183.
- Békésy GV (1952). Resting potentials inside the cochlear partition of the guinea pig. *Nature* **169**, 241–242.
- Békésy GV & Wever EG (1960). *Experiments in hearing*. McGraw-Hill, New York.
- Ben-Yosef T, Belyantseva IA, Saunders TL, Hughes ED, Kawamoto K, Van Itallie CM, Beyer LA, Halsey K, Gardner DJ, Wilcox ER, Rasmussen J, Anderson JM, Dolan DF, Forge A, Raphael Y, Camper SA & Friedman TB (2003). Claudin 14 knockout mice, a model for autosomal recessive deafness DFNB29, are deaf due to cochlear hair cell degeneration. *Hum Mol Genet* **12**, 2049–2061.
- Brownell WE, Spector AA, Raphael RM & Popel AS (2001). Micro- and nanomechanics of the cochlear outer hair cell. *Annu Rev Biomed Eng* **3**, 169–194.
- Dallos P (1985). Response characteristics of mammalian cochlear hair cells. *J Neurosci* **5**, 1591–1608.
- Dallos P, Santos-Sacchi J & Flock A (1982). Intracellular recordings from cochlear outer hair cells. *Science* **218**, 582–584.
- Davis H (1953). Energy into nerve impulses: the inner ear. *Adv Sci* **9**, 420–425.
- Davis H (1957). Biophysics and physiology of the inner ear. *Physiol Rev* **37**, 1–49.
- Davis H (1958). A mechano-electrical theory of cochlear action. *Ann Otol Rhinol Laryngol* **67**, 789–801.
- Davis H (1961). Some principles of sensory receptor action. *Physiol Rev* **41**, 391–416.
- Davis H (1965). A model for transducer action in the cochlea. *Cold Spring Harb Symp Quant Biol* **30**, 181–190.
- Davis H, Deatherage BH, Eldredge DH & Smith CA (1958). Summating potentials of the cochlea. *Am J Physiol* **195**, 251–261.
- Fernandez C (1952). Dimensions of the cochlea (guinea pig). *J Acoust Soc Am* **24**, 519–523.
- Fettiplace R (2017). Hair cell transduction, tuning, and synaptic transmission in the mammalian cochlea. *Compr Physiol* **7**, 1197–1227.
- Hibino H, Horio Y, Inanobe A, Doi K, Ito M, Yamada M, Gotow T, Uchiyama Y, Kawamura M, Kubo T & Kurachi Y (1997). An ATP-dependent inwardly rectifying potassium channel, K(AB)-2 (Kir4.1), in cochlear stria vascularis of inner ear: its specific subcellular localization and correlation with the formation of endocochlear potential. *J Neurosci* **17**, 4711–4721.
- Hibino H & Kurachi Y (2006). Molecular and physiological bases of the K<sup>+</sup> circulation in the mammalian inner ear. *Physiology* **21**, 336–345.
- Hibino H, Nin F, Tsuzuki C & Kurachi Y (2010). How is the highly positive endocochlear potential formed? The specific architecture of the stria vascularis and the roles of the ion-transport apparatus. *Pflugers Arch* **459**, 521–533.
- Hinojosa R & Rodriguez-Echandia EL (1966). The fine structure of the stria vascularis of the cat inner ear. *Am J Anat* **118**, 631–663.
- Hirose K & Liberman MC (2003). Lateral wall histopathology and endocochlear potential in the noise-damaged mouse cochlea. *J Assoc Res Otolaryngol* **4**, 339–352.
- Honrubia V & Ward PH (1968). Longitudinal distribution of the cochlear microphonics inside the cochlear duct (guinea pig). *J Acoust Soc Am* **44**, 951–958.
- Honrubia V & Ward PH (1969). Properties of the summating potential of the guinea pig's cochlea. *J Acoust Soc Am* **45**, 1443–1450.
- Hudspeth AJ (1989). How the ear's works work. *Nature* **341**, 397–404.
- Hudspeth AJ (1997). How hearing happens. *Neuron* **19**, 947–950.
- Hudspeth AJ (2008). Making an effort to listen: mechanical amplification in the ear. *Neuron* **59**, 530–545.
- Ikeda K & Morizono T (1989). Electrochemical profiles for monovalent ions in the stria vascularis: cellular model of ion transport mechanisms. *Hear Res* **39**, 279–286.
- Jacob S, Pienkowski M & Fridberger A (2011). The endocochlear potential alters cochlear micromechanics. *Biophys J* **100**, 2586–2594.
- Kennedy HJ, Evans MG, Crawford AC & Fettiplace R (2003). Fast adaptation of mechano-electrical transducer channels in mammalian cochlear hair cells. *Nat Neurosci* **6**, 832–836.
- Kikuchi T, Adams JC, Miyabe Y, So E & Kobayashi T (2000a). Potassium ion recycling pathway via gap junction systems in the mammalian cochlea and its interruption in hereditary nonsyndromic deafness. *Med Electron Microsc* **33**, 51–56.
- Kikuchi T, Kimura RS, Paul DL & Adams JC (1995). Gap junctions in the rat cochlea: immunohistochemical and ultrastructural analysis. *Anat Embryol (Berl)* **191**, 101–118.
- Kikuchi T, Kimura RS, Paul DL, Takasaka T & Adams JC (2000b). Gap junction systems in the mammalian cochlea. *Brain Res Rev* **32**, 163–166.
- Kilkenny C, Browne WJ, Cuthill IC, Emerson M & Altman DG (2010). Improving bioscience research reporting: the ARRIVE guidelines for reporting animal research. *PLoS Biol* **8**, e1000412.
- Konishi T & Salt AN (1983). Electrochemical profile for potassium ions across the cochlear hair cell membranes of normal and noise-exposed guinea pigs. *Hear Res* **11**, 219–233.
- Kubisch C, Schroeder BC, Friedrich T, Lütjohann B, El-Amraoui A, Marlin S, Petit C & Jentsch TJ (1999). KCNQ4, a novel potassium channel expressed in sensory outer hair cells, is mutated in dominant deafness. *Cell* **96**, 437–446.
- Michalski N & Petit C (2019). Genes involved in the development and physiology of both the peripheral and central auditory systems. *Annu Rev Neurosci* **42**, 67–86.
- Nin F, Hibino H, Doi K, Suzuki T, Hisa Y & Kurachi Y (2008). The endocochlear potential depends on two K<sup>+</sup> diffusion potentials and an electrical barrier in the stria vascularis of the inner ear. *Proc Natl Acad Sci U S A* **105**, 1751–1756.
- Nin F, Hibino H, Murakami S, Suzuki T, Hisa Y & Kurachi Y (2012). Computational model of a circulation current that controls electrochemical properties in the mammalian cochlea. *Proc Natl Acad Sci U S A* **109**, 9191–9196.

- Nin F, Yoshida T, Murakami S, Ogata G, Uetsuka S, Choi S, Doi K, Sawamura S, Inohara H, Komune S, Kurachi Y & Hibino H (2017). Computer modeling defines the system driving a constant current crucial for homeostasis in the mammalian cochlea by integrating unique ion transports. *NPJ Syst Biol Appl* **3**, 24.
- Nin F, Yoshida T, Sawamura S, Ogata G, Ota T, Higuchi T, Murakami S, Doi K, Kurachi Y & Hibino H (2016). The unique electrical properties in an extracellular fluid of the mammalian cochlea; their functional roles, homeostatic processes, and pathological significance. *Pflugers Arch* **468**, 1637–1649.
- Ogata G, Ishii Y, Asai K, Sano Y, Nin F, Yoshida T, Higuchi T, Sawamura S, Ota T, Hori K, Maeda K, Komune S, Doi K, Takai M, Findlay I, Kusuhara H, Einaga Y & Hibino H (2017). A microsensing system for the in vivo real-time detection of local drug kinetics. *Nat Biomed Eng* **1**, 654–666.
- Ota T, Nin F, Choi S, Muramatsu S, Sawamura S, Ogata G, Sato MP, Doi K, Doi K, Tsuji T, Kawano S, Reichenbach T & Hibino H (2020). Characterisation of the static offset in the travelling wave in the cochlear basal turn. *Pflugers Arch* **472**, 625–635.
- Patuzzi R (2011). Ion flow in stria vascularis and the production and regulation of cochlear endolymph and the endolymphatic potential. *Hear Res* **277**, 4–19.
- Robertson D & Johnstone BM (1980). Acoustic trauma in the guinea pig cochlea: early changes in ultrastructure and neural threshold. *Hear Res* **3**, 167–179.
- Salt AN & Konishi T (1979). Effects of noise on cochlear potentials and endolymph potassium concentration recorded with potassium-selective electrodes. *Hear Res* **1**, 343–363.
- Salt AN, Melichar I & Thalmann R (1987). Mechanisms of endocochlear potential generation by stria vascularis. *Laryngoscope* **97**, 984–991.
- Sato M, Baumhoff P & Kral A (2016). Cochlear implant stimulation of a hearing ear generates separate electro-phonic and electroneural responses. *J Neurosci* **36**, 54–64.
- Schmiedt RA, Lang H, Okamura HO & Schulte BA (2002). Effects of furosemide applied chronically to the round window: a model of metabolic presbycusis. *J Neurosci* **22**, 9643–9650.
- Smith CA, Lowry OH & Wu M-L (1954). The electrolytes of the labyrinthine fluids. *Laryngoscope* **64**, 141–153.
- Spicer SS & Schulte BA (1996). The fine structure of spiral ligament cells relates to ion return to the stria and varies with place-frequency. *Hear Res* **100**, 80–100.
- Spicer SS & Schulte BA (1998). Evidence for a medial K<sup>+</sup> recycling pathway from inner hair cells. *Hear Res* **118**, 1–12.
- Takeuchi S & Ando M (1998). Dye-coupling of melanocytes with endothelial cells and pericytes in the cochlea of gerbils. *Cell Tissue Res* **293**, 271–275.
- Takeuchi S, Ando M & Kakigi A (2000). Mechanism generating endocochlear potential: role played by intermediate cells in stria vascularis. *Biophys J* **79**, 2572–2582.
- Tasaki I & Spyropoulos CS (1959). Stria vascularis as source of endocochlear potential. *J Neurophysiol* **22**, 149–155.
- Thalmann R, Miyoshi T & Thalmann I (1972). The influence of ischemia upon the energy reserves of inner ear tissues. *Laryngoscope* **82**, 2249–2272.
- Wada J, Paloheimo S, Thalmann I, Bohne BA & Thalmann R (1979). Maintenance of cochlear function with artificial oxygen carriers. *Laryngoscope* **89**, 1457–1473.
- Wang Y, Hirose K & Liberman MC (2002). Dynamics of noise-induced cellular injury and repair in the mouse cochlea. *J Assoc Res Otolaryngol* **3**, 248–268.
- Wangemann P (2002). K<sup>+</sup> cycling and the endocochlear potential. *Hear Res* **165**, 1–9.
- Wangemann P (2006). Supporting sensory transduction: cochlear fluid homeostasis and the endocochlear potential. *J Physiol* **576**, 11–21.
- Weber PC, Cunningham CD & Schulte BA (2001). Potassium recycling pathways in the human cochlea. *Laryngoscope* **111**, 1156–1165.
- Yoshida T, Nin F, Murakami S, Ogata G, Uetsuka S, Choi S, Nakagawa T, Inohara H, Komune S, Kurachi Y & Hibino H (2016). The unique ion permeability profile of cochlear fibrocytes and its contribution to establishing their positive resting membrane potential. *Pflugers Arch* **468**, 1609–1619.
- Yoshida T, Nin F, Ogata G, Uetsuka S, Kitahara T, Inohara H, Akazawa K, Komune S, Kurachi Y & Hibino H (2015). NKCCs in the fibrocytes of the spiral ligament are silent on the unidirectional K<sup>+</sup> transport that controls the electrochemical properties in the mammalian cochlea. *Pflugers Arch* **467**, 1577–1589.
- Zdebek AA, Wangemann P & Jentsch TJ (2009). Potassium ion movement in the inner ear: insights from genetic disease and mouse models. *Physiology(Bethesda)* **24**, 307–316.
- Zidanic M & Brownell WE (1990). Fine structure of the intracochlear potential field. I. The silent current. *Biophys J* **57**, 1253–1268.

## Additional information

### Data availability statement

The data that support the findings of this study are available within the paper and its Supplementary Information uploaded to figshare (for URLs, see text). Additional data are available from the corresponding author upon reasonable request.

### Competing interests

The authors declare no competing financial interests.

### Author contributions

F.N., K.D., A.H. and H.H. designed the experiments and simulation. Q.Z. carried out the *in vivo* measurements. T.Y., D.I. and M.P.S developed the experimental setup. T.O. performed the simulation. T.Y. and A.H. supported the data collection. Q.Z., T.O. and D.I. analysed the data. T.Y, F.N. and H.H. wrote the paper. All authors edited the paper.

### Funding

This work was supported by the following research grants and funds: AMED-CREST JP20gm0810004 (to H.H.) from AMED, Grant-in-Aid for Scientific Research A 18H04062 (to H.H.), Grant-in-Aid for Challenging Exploratory Research 20K21883 (to H.H.), Grant-in-Aid for Early-Career Scientists 20K20164 (to T.O.) and 19K18824 (to M.P.S), and Grant-in-Aid for Scientific Research C 21K09642 (to K.D.), from the Ministry of Education, Culture, Sports, Science and Technology of Japan.

### Acknowledgements

The authors thank T. Tsuchida and S. Kuwabara for their technical assistance.

### Keywords

acoustic stimulation, circulation current, electrical circuit, hair cells, stria vascularis

### Supporting information

Additional supporting information can be found online in the Supporting Information section at the end of the HTML view of the article. Supporting information files available:

### Peer Review History

### Statistical Summary Document